The variation of sinter strength in the sinter bed due to the mineral phase distribution

by

Willem Jacobus Jordaan

Submitted in partial fulfilment of the requirements for the Degree of Masters in Engineering in the Faculty of Engineering, the Built Environment and Information Technology University of Pretoria

2002-07-10

The variation of sinter strength in the sinter bed due to the mineral phase distribution

By: Willem Jacobus Jordaan

Supervisor: Prof. J.M.A. Geldenhuis

Co-supervisor: Prof. P.C. Pistorius

Department of Materials Science and Metallurgical Engineering

Masters in Metallurgical Engineering

It is well known that the quality of sinter is mainly governed by the microstructure and phase composition of the sinter. The phase composition through the sinter bed varies because the sintering conditions are not the same through the sinter bed. Sintering conditions are determined by the temperature-time-characteristics of the sintering process. The aim of this investigation was to investigate the influence that the temperature-time-characteristics of the sinter process may have on the phase formation and sinter quality.

Two series of sinter pot tests were conducted at a different pressure drop over the sinter bed. In the first series the pressure drop was maintained at 1100mmH_2O during the sintering and cooling stage of the sinter process. In order to increase the airflow rate through the sinter bed the pressure drop over the sinter bed was increased to 1500mmH_2O during the second series of sinter pot tests. Data was recorded to determine the temperature profiles in the top, middle and bottom layer of the sinter bed and to determine the temperature-time-characteristics of the sintering process at the different airflow rates.

The sinter cakes produced in each series were divided into three layers to form a top, middle and bottom layer. The physical properties of each layer were quantified with the tumbler test and sieve analyses. A mineralogical study was conducted on each

layer to determine the phase composition. The chemical composition of each phase was determined and the stoichiometry of the relevant phases was calculated.

Because of the different temperature-time-characteristics of the different layers the phase composition and morphology differ in each layer. The longer the sintering time the more hematite is reduced to magnetite. Therefore, the higher magnetite content in the middle and bottom layer. The resulting hematite content correlates with the magnetite content. The higher the magnetite content the lower is the hematite content. A longer sintering time at temperatures higher than 1100°C results in a higher SFCA content. The SFCA content increased from the top layer to the bottom layer. The silica glass content decreased from the top layer to the bottom layer. Linked to these changes in phase content the sinter strength increased from the top layer to the bottom layer.

This project revealed that the sintering time above the temperature of 1100°C is one of the most important parameters to ensure that phases that will enhance sinter quality are formed. The sintering time above 1100°C increased from the top layer to the bottom layer. The sintering time above 1100°C also increased at a lower airflow rate through the sinter bed in series one resulting in a lower magnetite and higher SFCA content and improved sinter quality.

In spite of the correlation found between the sinter strength and phase composition of the sinter in this investigation, it became clear that the phases are not the only parameter determining the sinter strength. The morphology of the sinter phases present, porosity of the sinter and coke rate may have an influence on the sinter quality and should be investigated.

Key words:
Sinter, sinter bed, phase composition, microstructure, physical properties, temperature profile

ACKNOWLEDGEMENTS

I would like to thank the following persons and institutions:

- Prof. J.M.A. Geldenhuis (mentor) and Prof. P.C. Pistorius (co-mentor) of the University of Pretoria for their advice and expertise that contribute to the successful completion of this project.
- Prof. A. Carbers-Craig of the University of Pretoria for the detailed phase analyses performed on the sinter.
- Personnel at Iscor Technology for advice and their contribution with regard to this project.
- Iscor Technology for the opportunity to perform the test work on this project at their research facilities.

TABLE OF CONTENTS

TABLE OF CONTENTS (continue)

LIST OF ILLUSTRATIONS

List of figures Page

LIST OF ILLUSTRATIONS (continue)

List of figures Page

List of tables Page

1. INTRODUCTION

It is well known that the quality of sinter is mainly governed by the microstructure and phase composition of the sinter. The bonding phases make up the majority of phases within sinter (up to 80vol%). These phases are formed during the sinter process at temperatures above 1100°C. Therefore, the temperature-time-characteristics of the sinter process is an important parameter that contributes to the microstructure and phase composition of sinter. The sintering conditions are not the same through the sinter bed. This will result in a variation in the phase composition through the sinter bed. The aim of this investigation was to investigate the influence that the temperature-time-characteristics of the sinter process may have on phase formation and the sinter quality.

2. LITERATURE REVIEW

2.1 SINTER PROCESS DESCRIPTION

Sintering is a generic term that is used to describe a high temperature process in which a raw materials mixture is converted into a particular form of agglomerate known as sinter[1].

On a production plant the sintering process is divided into several sub-processes[1]:

- Blending and granulation of the sinter mixture.
- Charging into sinter cars in the sinter machine to form a sinter bed.
- Ignition of the fuel in the surface of the bed.
- Sequential combustion of the fuel in horizontal layers.
- Reaction at high temperatures involving the liquid melt and solids.
- Cooling and solidification of the melt.
- Crushing of the agglomerate to obtain a manageable size distribution.

Iron ore fines, coke breeze, flux and other raw materials are mixed together. Water is added to the mixture. The mixture is then granulated into pseudo-particles in a rotary mixer. Granulation involves the layering of fine particles (<0.25mm) onto the surface

of coarser particles (>1mm). Therefore, the pseudo-particle consists of a coarse nucleus particle and fine particles attached to the nucleus particle. Particles in the range between, called intermediate fines, remain detached and find their way into the voids of the sinter bed. Good granulation coarsens the mix and narrows the size distribution.

The purpose of granulation is to improve the bed permeability that will enhance the flow characteristics of the combustion air through the sinter bed. This will contribute to improved sinter quality and productivity. During sintering the permeability of the sinter bed is adequately maintained because large nucleus particles remain unmelted. The voids between the pseudo-particles will collapse and the permeability of the sinter bed will consequently decrease if there are no such nucleus particles at all[2]. A binder such as quick lime may be added during the granulation process to help to keep the microstructure of the pseudo-particles stable when moisture is removed during sintering.

The granulated mixture is charged onto a grid layer of coarse sinter (-40+20mm) in sinter cars on the sinter machine. The height of the packed bed varies from process to process and can be up to 600mm in height. The bed immediately passes under an ignition hood where the fine coke in the surface layer is ignited by gas flames. As the sinter cars move forward, combustion is promoted by air drawn through the sinter bed into a series of wind boxes under the sinter bed. The pressure drop over the sinter bed can be up to 2000mm H_2O[3].

In the sintering process the temperature of the granulated sinter mixture is raised to temperatures between 1250°C and 1400°C to achieve partial fusion. During the heating and cooling cycle different species react with each other to produce certain phases. Molten material is produced which crystallises or solidifies into various phases that bond the microstructure together[4]. Therefore, sinter consists of an assembly of various phases such as hematite, magnetite, SFCA and calcium silicate of varying chemical composition and morphology. Each of the different phases has a unique influence on the sinter quality.

The sinter cake is either cooled on the sinter strand (on-strand cooling) or outside the sintering machine (off-strand cooling). The sinter is crushed and screened to a size range desirable as a blast furnace feed for example -50+5mm.

2.2 SINTERING ZONES

The sinter mixture is subjected to different thermal and physical conditions during sintering. It is therefore possible to divide the sinter bed into different zones that coexist during the sintering process (**Figure 1**). Each of the zones has a profound influence on sintering performance and sinter quality[5].

When the bed is sectioned vertically it is evident that combustion is confined to a thin layer between unsintered feed below and cooling sinter above[6]. This layer is known as the combustion layer (**Figure 1**). The combustion layer travels at 1cm/min to 3cm/min towards the grate[7].

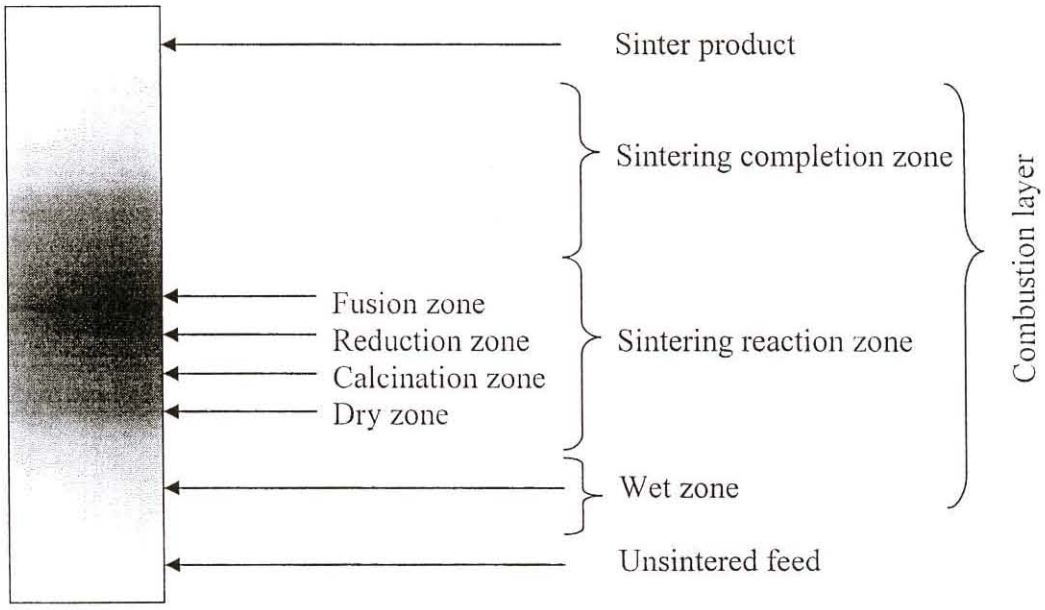

Figure 1: Sintering zones

As combustion proceeds through the sinter bed each part of the sinter bed is subjected to a characteristic temperature cycle. The temperature rapidly increases to a maximum temperature and remains there for a few minutes. As the combustion layer moves further down the sinter bed the material cools down with time.

Fundamentally sintering is an efficient heat transfer process in which heat is continually transferred downward through the bed[6]. Air entering the bed is heated by the warm sinter above the combustion layer and attains its peak temperature in the combustion layer. The gas leaving the combustion layer transfers heat to the feed below. The gas serves to ignite the coke breeze and to initiate endothermic changes and reactions[6].

The combustion layer consists of the following zones[2] (**Figure 1**):

- A wet zone.
- A sintering reaction zone.
- A sintering completion zone.

2.2.1 THE WET ZONE

The lower part of the sinter bed acts as de-humidifier and removes water from the flowing air. The accumulation of water in this part of the sinter bed results in the wet zone. The start of the wet zone is often well defined because of the presence of a thin layer of fines[5]. These fines have been detached from pseudo-particles in the sintering reaction zone and have been captured by the wet zone. Their presence will definitely increase the resistance of the wet zone to air flow[5]. As the combustion layer moves down so will this layer of fine captured particles. The wet zone basically acts as a very effective wet scrubber for fine particles. It is most likely that other material, e.g. volatilised alkali chlorides, could also be scrubbed out in the wet zone[5]. The wet zone disappears when the combustion layer has moved low enough down the sinter bed. The accumulated layer of fines and dissolved substances will leave the sinter bed in the off-gas[5].

2.2.2 THE SINTERING REACTION ZONE

The height of the sintering reaction zone is approximately 70mm and the reaction time in this zone is 3min[2]. Various changes occur in this zone as the temperature rises and also during cooling. It is assumed that the process is complete when the temperature drops below 1100°C[4]. The following processes occur in the sintering reaction zone[4]:

- Solid state reactions.
- Melting of the products to form a primary liquid.
- Dissolution of solids in the melt to form a secondary liquid.
- Crystallization of the phases from the liquid on cooling.
- Solidification of the liquid to form glass.

The sintering reaction zone is further divided into the following zones[2] (**Figure 1**):

- Dry zone.
- Calcination zone.
- Reduction zone.
- Fusion zone.

(a) THE DRY ZONE

Due to the downward movement of the combustion layer the mixture in front of the combustion layer is dried by the heat from the warm gas leaving the combustion layer.

(b) THE CALCINATION ZONE

The temperature has increased to a point where calcination of some of the raw materials for example dolomite may occur.

(c) THE REDUCTION ZONE

The combustion of coke begins between 700°C and 800°C[2]. With increasing temperature the CO_2-gas reacts with the coke to produce CO-gas. The CO-gas reduces hematite to produce magnetite. When further reduction occurs wustite is formed.

(d) THE FUSION ZONE

In the fusion zone reactions occur at high temperatures and are termed sintering reactions. These reactions determine the mineralogy and texture of the sinter and consequently the sinter properties[1]. The reactions are extremely complex, involving physical and chemical factors of which many are inherent properties of the raw materials used.

2.2.3 THE SINTER COMPLETION ZONE

Crystallisation and solidification occur on cooling. Final reactions between the different phases and chemical species result in the final phase composition and microstructure of the sinter.

2.3 THE TEMPERATURE PROFILE AND HEAT INPUT

The temperature profile in the sinter bed is schematically shown in **Figure 2**. This profile is characterised by a steep rise to a maximum temperature (T_{max}) during the heating cycle. It takes normally about two minutes[8] to heat the raw materials to maximum temperature. The maximum temperature reached is often higher than 1300°C and may be as high as 1350°C[9]. The maximum temperature reached depends mainly on the quantity, location, amount of coke used and the combustibility of the coke[4].

The depth of the bed and airflow rate also have a significant effect on the maximum temperature reached. A gentle slope after reaching maximum temperature indicates the relatively slow cooling of the finished sinter during the cooling cycle. The time to cool to room temperature is a function of the maximum temperature[6]. As the maximum temperature increases the time to cool down will also increase.

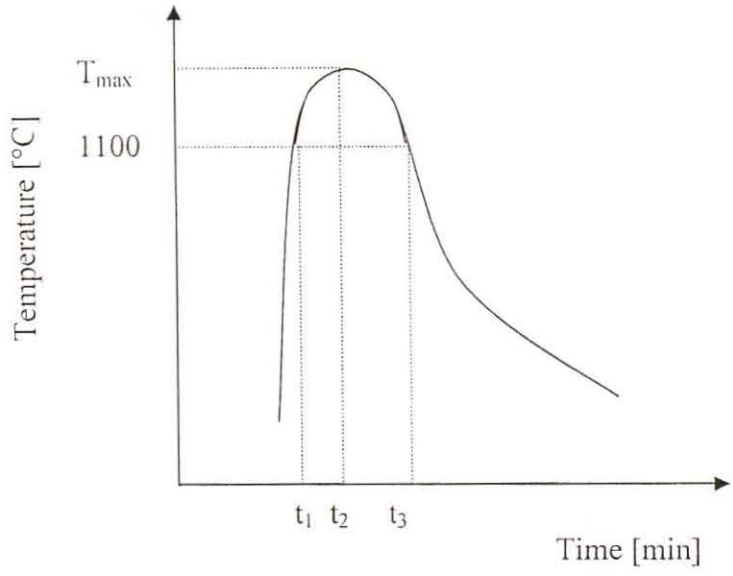

Figure 2: A schematic diagram of a typical temperature profile in a sinter bed

Energy is supplied during sintering when heat is continually transferred downward through the bed. The quantity that is continually transferred is equivalent to the sensible heat of the bed itself once the process is fully established[6]. The supplied energy will increase when the time at temperatures higher than 1100°C (t_3-t_1) increases (**Figure 2**).

Different temperature profiles are obtained from top to bottom in the sinter bed. Both the maximum temperature and the area below the temperature profile vary from top to bottom. The maximum temperature is lower and the retention time at the maximum temperature is shorter in the top layer than in the bottom layer[10]. To improve the microstructure of the sinter it is important to minimise the difference in temperature profile and to control it to a suitable heat pattern[10]. Because of these differences the discharged sinter may be classified as follows[6]:

1. Top sinter: generally weak and friable giving a poor yield of sinter with an acceptable size grading. This sinter is fused at a high temperature and chilled immediately thereafter. The sinter is discharged cold from the sinter strand.

2. Middle sinter: This sinter is formed under optimum conditions for fusion and annealing and gives the maximum yield of sinter with acceptable size grading. The sinter is discharged cold from the sinter strand.
3. Bottom sinter: This sinter is discharged hot and is chilled severely as it passes through the breaker and over the discharge screen onto the cooler. This may result in poor physical properties giving a lower yield of sinter with acceptable size grading. If on-strand cooling applies, the sinter will have almost the same properties as the sinter in the middle layer.

2.4 MICROSTRUCTURE

Two types of sinter microstructure can be produced depending on the sintering conditions, in particular the sintering temperature[4]:

A homogeneous microstructure implies that the visual appearance of the sinter is homogeneous. Homogeneous sinter is produced at higher sintering temperatures (T>1300°C) and usually contains only precipitated phases.

A heterogeneous microstructure implies that the visual appearance of the sinter is heterogeneous in which a significant amount of large particles remains partially unreacted. This microstructure is produced at T<1300°C. An important characteristic of such sinters is the presence of unreacted ore particles[11].

2.5 PHASES

The main phases occurring in sinter are SFCA, unassimilated iron ore particles, precipitated oxides of iron (magnetite and hematite) and dicalcium silicate as matrix[2][12]. In a study on South African sinters by PA Botha[13] phases like hematite, magnetite, SFCA and calcium silicate were examined. This study revealed that hematite, magnetite and SFCA dominated in the sinter investigated with small quantities of calcium silicate, glass, periclase, wustite and manganosite[13].

2.5.1 HEMATITE

Three types of hematite commonly occur in sinters namely massive hematite, crystalline hematite and secondary hematite[13]. Massive hematite is hematite originating from iron ore particles that did not fully participate in the sintering reactions. Massive hematite remains partly in its original state.

Crystalline hematite precipitates from the melt[12]. Crystalline hematite may exist at the periphery of the massive hematite particles. Crystallization occurs in the presence of oxygen usually near cracks and pores[13].

Oxidation of magnetite to hematite may occur during cooling of the sinter in air[13]. The resulting phase is called secondary hematite. Secondary hematite is usually found around the edges of open pores in sinter[12].

2.5.2 MAGNETITE

Magnetite is formed on crystallisation from the melt or solid state reduction of hematite or solid state oxidation of wustite. However, it is rare to find unassimilated magnetite in sinter. The magnetite precipitates from the melt as a spinel and contains small amounts of Mg, Si, Ca and Mn together with a variable but relatively small amount of Al[12].

2.5.3 SFCA

The most common ferrite found in sinter is more accurately described as silico-ferrites of calcium and aluminium (SFCA)[12]. It contains significant amounts of silicon and aluminium as well as calcium and iron. This phase may vary considerably in composition and morphology[12].

The term SFCA that is used in sintering refers to a wide range of compounds. **Table 1** gives examples of typical compounds in different systems[14].

Table 1: SFCA

System	Compound
Binary system	$CaO\text{-}Fe_2O_3$
Ternary system	$CaO\text{-}Al_2O_3\text{-}Fe_2O_3$
Quaternary system	$CaO\text{-}Al_2O_3\text{-}SiO_2\text{-}Fe_2O_3$
SFCA	$7Fe_2O_3.2SiO_2.3Al_2O_3.5CaO$ $9Fe_2O_3.2SiO_2.0.5Al_2O_3.5CaO$
SFCA general	$xFe_2O_3.ySiO_2.zAl_2O_3.5CaO$ where x+y+z=12

Dendritic SFCA is the first type of SFCA that is formed during the sintering process[13]. Dendritic crystals are very small, usually smaller than 4μm. Crystal growth between 1200°C and 1300°C results in bigger crystals called acicular SFCA[13]. The crystals of acicular SFCA are larger than 4μm but smaller than 10μm. During the heating cycle acicular SFCA melts at 1300°C and will precipitate as columnar SFCA during the subsequent cooling cycle. These are rather large crystals with a typical size of 10μm and larger[13].

SFCA is the product of several successive reactions[14]:

1. The formation of monocalcium ferrite at temperatures from 1050°C to 1150°C.
2. The reaction between Al_2O_3 and CaO to produce calcium aluminate (1100°C-1150°C).
3. Dissolution of the calcium aluminate in monocalcium ferrite at 1100°C-1150°C to produce aluminous monocalcium ferrite.
4. Fusion of the aluminous monocalcium ferrite and reaction with Fe_2O_3 at 1200°C-1250°C to produce aluminous hemicalcium ferrite.
5. Reaction with SiO_2 at 1200°C-1250°C to produce SFCA.

Aluminium stabilises SFCA. The SFCA requires a critical level of ±3% aluminium to stabilise the phase[12]. At lower levels magnetite and dicalcium silicate are formed. There is a relatively constant ratio of calcium to silicon atoms close to two in this phase. The iron is in the ferric state[12].

2.5.4 CALCIUM SILICATE

Glassy silicate, often referred to as slag phases, is formed when the melt from which primary phases have precipitated is rapidly cooled[2]. The most common silicate is based on dicalcium silicate but with varying amounts of calcium being replaced by iron[12].

2.6 PHASE FORMATION

2.6.1 SINTERING MECHANISM

An iron ore granule consists of a large iron ore core particle or nucleus with a layer or coating of adhering fines when charged to the sinter bed. The layer of fines consists of highly reactive ore particles, fluxes and other raw materials that are in intimate contact. Therefore, it is assumed that the sintering reactions will begin within the layer of adhering fines[1].

Combustion of fine coke particles starts at temperatures between 700°C and 800°C and results in the formation of CO gas. The nucleus surface and the adhering fines of the pseudo-particle are reduced by the CO gas into magnetite.

As the temperature rises to 1100°C low melting point phases such as Fe_2O_3-CaO, FeO-CaO and FeO-SiO_2 are formed by solid-solid phase reaction between CaO and Fe_2O_3[2][4]. SFCA and calcium silicate are formed in association with magnetite. Dicalcium silicate forms at 1150°C[4]. Complex SFCA is formed with silicate in solid solution.

During the heating cycle the formation of SFCA from the reaction between hematite and lime is the first reaction taking place. Al_2O_3 increases the dissociation temperature of SFCA and stabilises the phase as a result. Acicular SFCA starts to form below 1185°C[4]. With an increase in temperature to 1220°C much more acicular SFCA is generated[4]. The sinter mainly contains acicular SFCA and unreacted hematite at this stage.

When the temperature has risen to 1245°C the unreacted hematite disappears and the SFCA increases in crystal size[4]. Some granular magnetite grains grow in the SFCA microstructure. The magnetite grains are formed from the dissociation of SFCA. Some aggregated magnetite grains is also formed from the reduction of the unreacted hematite.

The SFCA begins to decompose when the temperature exceeds 1300°C[2][4]. At decomposition it will change to hematite when the partial pressure of oxygen is high and the temperature is lower than 1350°C. It will change to magnetite when the partial pressure of oxygen is low and the temperature is higher than 1350°C[2]. The proportion of SFCA that is decomposed may increase when the time of exposure above the decomposition temperature increases or when the maximum temperature that is reached during sintering increases. Therefore, the sinter will contain less SFCA and more magnetite and calcium silicate. At a high oxygen potential the sinter will contain less SFCA and more hematite and calcium silicate[8]. The slag components are distributed into the melt. On cooling, the magnetite transforms to coarse skeletal rhombohedral hematite. The SFCA grows to large columnar shaped crystals. The acicular SFCA may also decompose to hematite at a high oxygen partial pressure[2]. If the maximum temperature does not exceed 1300°C or the residence time at high temperature is low the sinter will be composed of acicular SFCA with silicate in solid solution and unreacted hematite ore particles[2][4].

A low melting point slag forms at ±1200°C and Al_2O_3-bearing phases dissolve into the slag melt[1][4]. The hematite grain boundaries are broken by the penetration of the slag melt. The process is termed nucleus assimilation[1]. Assimilation of the unreacted hematite particles will produce magnetite and acicular SFCA with silicate in solid solution[2][4]. The following mechanism is proposed[10]:

1. The surface of the hematite particle is reduced to magnetite.
2. The magnetite reacts with the silicate melt and oxygen to produce SFCA.
3. The above reactions continue and penetrate through the hematite particle.

The degree of assimilation depends on the properties of the initial melt and nucleus. The greater the reactivity of the melt, the greater its ability to digest the solid nucleus. The greater the assimilation resistance of the solid nucleus, the less the amount that

would be assimilated. Assimilation starts with the local formation of a primary liquid phase that dissolves the bulk of the solid nucleus[15]. Liquid formation is promoted by the presence of fine-grained fusible and well-blended materials in the mixture.

During assimilation the slag elements diffuse selectively into the solid nucleus or iron ore crystals and influence their melting behavior[15]. The liquid slag penetrates between the oxide crystals and fills up holes and cavities. During this penetration the slag becomes more and more acid and rich in iron. The diffusion of calcium oxide into the magnetite lattice lowers the melting point of magnetite significantly. This phenomenon accelerates iron ore dissolution[15]. Calcium ions diffuse into the magnetite lattice during penetration of the liquid slag while iron ions diffuse into the liquid slag. Magnesium and aluminum ions also diffuse into the magnetite lattice[15].

The assimilation process terminates when the temperature of the melt surrounding the nucleus drops below the liquidus temperature due to the saturation of the melt by FeO or when the sintering temperature drops sufficiently to cause solidification of the melt or when the nucleus is completely assimilated[1].

Magnetite precipitates on resolidification and cooling. This phase contains Mg, Ca, Al and Si ions. Mg ions preferably dissolve in magnetite rather than in other phases[15]. An increasing MgO input will increase the magnetite spinel phase and consequently decreases the amount of hematite. Although the saturation concentration of MgO is much higher than CaO in magnetite, the CaO concentration of the mix exceeds that of MgO by far[15]. Therefore, the CaO content of the magnetite is generally higher than the MgO content. This leads to a decrease in the CaO content of the residual liquid phase when magnetite forms. When magnetite is cooled at a low rate and brought into contact with oxygen, it could also transform to hematite[2]. Hematite generally precipitates after magnetite formation.

SFCA precipitates at lower temperatures after magnetite and hematite[14]. SFCA crystallises from the melt and grows from small and thin columnar to large and columnar shaped SFCA[2]. If the maximum temperature does not exceed 1300°C during sintering or the residence time at the high temperature is extremely short, the microstructure of the sinter on cooling will be acicular SFCA with silicate in solid

solution and unmelted hematite ore particles[2]. In the cooling cycle it is possible for both hematite and magnetite to be resorbed by reaction with the silicate melt to form SFCA. This phenomenon is favoured by slow cooling and results in the formation of large crystals of SFCA, often in association with magnetite and glass[4]. Under reducing conditions magnetite is preserved and no SFCA is formed. However, under more oxidizing conditions magnetite is resorbed to produce SFCA. Calcium silicate instead of SFCA can form during rapid cooling[4].

The last phase that solidifies is the silicate melt as calcium silicate and glass[15].

2.6.2 EFFECT OF COKE CONSUMPTION

A high coke consumption (50-60kg/t) during the sintering process results in a typical microstructure[2] where columnar SFCA and magnetite co-exist surrounded by a relatively large amount of glassy silicate. A small number of fine pores exists in this microstructure. The magnetite is a multicomponent system and contains Al_2O_3, TiO_2 and MgO. Skeletal rhombohedral hematite is often formed in the vicinity of the large open pores. This hematite is produced by the transformation of magnetite during the cooling process. This type of microstructure is usually to be found in the lower part of the sintering bed where the maximum temperature was high and the cooling rate was low[2].

Another type of sinter microstructure is formed at a low coke consumption (40kg/t)[2]. Fine acicular SFCA is the main phase of this microstructure. The crystal growth is dense with small voids between the crystals that are relatively free of slag. This porous microstructure together with the type of SFCA result in a high reducibility of the sinter. No skeletal rhombohedral hematite is formed but unreacted ore particles exits in this microstructure surrounded by and/or penetrated by glassy silicate[2].

2.6.3 EFFECT OF OXYGEN POTENTIAL

The oxygen potential during the heating and cooling cycle will affect phase formation during the sintering process[8]. Material near coke particles is subjected to conditions of low oxygen potential during the heating cycle due to the combustion of the coke

particles and CO-gas formation[8]. Material adjacent to open pores is subjected to conditions of high oxygen potential during the cooling cycle due to the flow of air through the pores. Material further away from the pores is cooling at conditions of low oxygen potential[8].

During the heating stage SFCA transforms to hematite and silicate at a high oxygen potential. At a low oxygen potential it transforms to magnetite and silicate[8][10].

Magnetite near pores in the sinter microstructure is cooled under high oxygen potential conditions and tends to oxidise to hematite during the cooling stage. Magnetite cooling under conditions of lower oxygen potential will react with the silicate melt and oxygen to produce a large amount of columnar SFCA. If the region is near to coke it is cooled under low oxygen potential conditions. The magnetite will be preserved. This region will contain a large amount of magnetite[8][10].

It is concluded that with a decrease of the oxygen potential the magnetite content will increase but the SFCA content will decrease. The highest SFCA content is obtained at an intermediate level of oxygen potential[8].

2.7 SINTER QUALITY

Sinter quality refers to the physical and metallurgical properties of the sinter. The quality of sinter is usually defined in terms of:

- The physical strength of sinter at room temperature as measured by the shatter or tumbler test.
- Breakdown of sinter following reduction at low temperatures (550°C) determined by the reduction degradation test (RDI).
- Reducibility of the sinter determined by the reducibility test (RI) at 900°C.
- High temperature softening and melting properties of the sinter.

Sinter is an aggregate of bonding phases, unmelted particles and pores. Therefore, sinter quality is mainly governed by the microstructure and the phase composition of

the sinter. The size, shape, distribution and mutual interaction of the different phases present in the sinter are of great importance[16].

The sinter quality is also related to the temperature profile in the sinter bed during sintering[9]:

- The FeO content of the sinter is related to the maximum temperature.
- The reducibility increases if the area below the temperature curve decreases for temperatures above 1100°C. Therefore, the reducibility increases with decreasing heat input[4].
- The reduction disintegration properties of sinter deteriorate with faster cooling rate during the sintering process[4].
- Sinter strength increases with increasing area below the temperature curve for temperatures above 900°C.
- Sinter cold strength can be increased by increasing the coke rate up to some critical limit thereafter strength begins to fall[9].
- Reducibility increases as the amount of magnetite decreases[9].

2.7.1 PHYSICAL PROPERTIES

The individual phases of the sinter have a profound influence on the sinter strength[4]. The fracture toughness decreases from primary hematite to secondary hematite to magnetite to SFCA and finally to glass with the lowest strength[4].

The bonding phases (usually SFCA and calcium silicate) originate during the sintering process. The bonding phases make up the majority of phases within sinter (up to 80vol%)[12]. The sinter properties are therefore strongly related to the bonding phases. The phases are formed during the sinter process at temperatures above 1100°C. During cooling, internal tensions are developed because of the difference in shrinkage of the phases[6]. Cracking may occur that may lead to the breakdown of sinter particles.

The strength of sinter is determined by the size and shape of hematite, magnetite and SFCA which are dispersed in the glassy silicate matrix of the sinter[2]. The presence of

cracks in unassimilated hematite particles is the result of phase changes caused by oxidation or reduction. The reduction of hematite to magnetite during the sintering process is always associated with an apparent volume increase that may result in the formation of pores and cracks[12]. Secondary hematite particles do not appear to crack easily and this is thought to be a function of the smaller particle size[12]. SFCA is known to improve the sinter quality. The needle morphology of SFCA is heavily faulted and will arrest cracks. The porous microstructure of the ferrite can absorb stresses and prevents crack development[17].

Unmelted particles are mainly residual, large ore particles and sometimes unreacted residual flux particles. Since the sintering process is completed in a very short time the slag melt may not adequately surround the bigger unmelted particles. After cooling, the unmelted particles are not closely bonded by the surrounding bonding phases. Cracks will readily propagate through the weaker bond[2].

Sinter is a porous, brittle material. There is a wide variation in porosity, from open to closed and from macroscopic to microscopic. The porosity decreases with increasing sinter temperature[9]. The degree of breakage depends on the ease with which cracks propagate through the sinter particle. Sinter with many large open pores tends to break down more easily than sinter with a dense microstructure[2]. A high porosity may promote the transformation of hematite to magnetite during reduction[18] because the reduction gas easily accesses the porous sinter microstructure.

Sinter strength is determined by the sintering and annealing history of the sintering process[6]. To improve the cold strength of sinter sufficient retention time above 1100°C must be allowed. A residence time of 3-5min above 1100°C is recommended. This can be achieved by controlling the airflow through the bed which is a function of permeability, bed depth, strand speed and the pressure drop over the sinter bed[9].

Sinter strength also increases with increasing maximum temperature[9]. Experiments show that the sinter strength slightly increases with temperature up to 1275°C due to the increasing SFCA content[9]. It rapidly increases above this temperature due to densification and melt formation which were reflected by lower porosity and

increased glass content. Fine fibrous SFCA minimises the number of cracks and large pores and therefore improves the cold strength of the sinter[9].

2.7.2 REDUCTION DISINTEGRATION

The reduction disintegration index (RDI) of the sinter is determined by the ISO 4696 reduction disintegration test. The RDI is a quantitative measure of the degree of disintegration of the sinter that could occur in the upper part of the blast furnace after some reduction.

Breakdown as a result of reduction normally increases with the amount of reoxidised hematite in the sinter because of the transformation of hematite to magnetite during reduction at ±550°C[18]. Coarse secondary hematite (skeletal rhombohedral hematite) are the main cause of reduction degradation[4]. The formation of secondary hematite is minimised by lowering the maximum sinter temperature[9].

2.7.3 RI

The ISO 4695 reducibility test (RI) is one of several procedures used to evaluate the behaviour of sinter under specific conditions i.e. isothermal reduction, reduction in a fixed bed and reduction by means of carbon monoxide. The results of this test should be considered in conjunction with the RDI results.

Each phase in the sinter microstructure will respond according to its reduction behaviour when the sinter is reduced in the blast furnace[17]. The quantity of fine open pores and SFCA may increase the reducibility of the sinter. The reducibility may also vary with the morphology of the SFCA in the sinter. Experiments show that acicular SFCA is more reducible than columnar SFCA[2]. Acicular SFCA has a highly porous microstructure allowing good gas flow to the reaction surface. It is also chemically more reducible than the other morphologies of SFCA. The reducibility decreases as the density of SFCA increases when it becomes increasingly more columnar SFCA[4][9][16].

2.7.4 HIGH TEMPERATURE PROPERTIES

High temperature properties can be referred to as high temperature softening and melting properties of the sinter at reduction temperatures above 1100°C. An increasing sinter reducibility usually leads to better high temperature properties[4].

3. AIM OF THIS INVESTIGATION

The aim of this investigation was to investigate the influence that the temperature-time-characteristics of the sinter process may have on phase formation and the sinter quality.

By changing the airflow rate through the sinter bed it should be possible to change the temperature-time-characteristics of the sinter process. The temperature-time-characteristics should have an influence on the phase composition and morphology of the phases produced. The resulting effect on phase formation will be investigated. Sinter quality is strongly related to the phases present in the sinter. The correlation between the phases present and the sinter quality will be investigated.

According to literature it is important to minimise the difference in temperature profile and to control it to a suitable heat pattern to improve the microstructure of the sinter[10]. Because of the different temperature profiles in the different layers the discharged sinter has different physical properties. Sinter in the top layer is generally weak and friable giving a poor yield of sinter with an acceptable size grading and has therefore poor physical properties[6]. The sinter in the middle layer is formed under optimum conditions for fusion and annealing and gives the maximum yield of sinter with acceptable size grading and has therefore optimum physical properties[6]. If on-strand cooling applies, the sinter in the bottom layer will have almost the same properties as the sinter in the middle layer[6].

2.7.4 HIGH TEMPERATURE PROPERTIES

High temperature properties can be referred to as high temperature softening and melting properties of the sinter at reduction temperatures above 1100°C. An increasing sinter reducibility usually leads to better high temperature properties[4].

3. AIM OF THIS INVESTIGATION

The aim of this investigation was to investigate the influence that the temperature-time-characteristics of the sinter process may have on phase formation and the sinter quality.

By changing the airflow rate through the sinter bed it should be possible to change the temperature-time-characteristics of the sinter process. The temperature-time-characteristics should have an influence on the phase composition and morphology of the phases produced. The resulting effect on phase formation will be investigated. Sinter quality is strongly related to the phases present in the sinter. The correlation between the phases present and the sinter quality will be investigated.

According to literature it is important to minimise the difference in temperature profile and to control it to a suitable heat pattern to improve the microstructure of the sinter[10]. Because of the different temperature profiles in the different layers the discharged sinter has different physical properties. Sinter in the top layer is generally weak and friable giving a poor yield of sinter with an acceptable size grading and has therefore poor physical properties[6]. The sinter in the middle layer is formed under optimum conditions for fusion and annealing and gives the maximum yield of sinter with acceptable size grading and has therefore optimum physical properties[6]. If on-strand cooling applies, the sinter in the bottom layer will have almost the same properties as the sinter in the middle layer[6].

4. EXPERIMENTAL PROCEDURE

The sinter pot test was designed according to the requirements of real plant conditions. The sinter pot test can be conducted for several different purposes but the main aim is to evaluate the influence of different sinter mixture compositions on the quality of the sinter product. The results of the sinter pot test can also be used for sinter process optimisation. From the results of the sinter pot tests, the sintering behaviour of the raw materials in the sinter mixture are determined, typical quality measures being production rate, fuel consumption rate and sinter quality.

Representative samples of the different raw materials used in the sinter plant were obtained and prepared for sinter pot tests. The percentages of the different raw materials used in the sinter mixture are given in **Table 2**. The sinter mixture was composed in order to obtain a sinter with a FeO content of seven percent and basicity (CaO/SiO_2) of two. The sinter mixture and amount of water added were composed to achieve similar bed permeabilities. The dry raw materials were mixed together in a rotary mixer. The water was added and further mixing for six minutes resulted in adequate granulation.

Table 2: Sinter mixture

	Series 1 [mass %]	**Series 2** [mass %]
Pressure drop	1100mmH_2O	1500mmH_2O
Iron ore A	14.60	14.43
Iron ore B	18.77	18.55
Iron ore C	9.38	9.26
Return fines	28.83	28.61
Lime	2.68	3.62
Quick lime	1.99	1.99
Dolomite	5.10	4.89
Coke	3.23	3.23
Waste material mixture	9.79	9.79
Water	5.47	5.47
$CaCl_2$	0.16	0.16

The sinter pot was prepared with a grid layer consisting of –40+20mm sinter particles. The grid layer was 50mm in height. The raw materials were fed from the rotary mixer

into the sinter pot with a conveyer system. The total bed height was 500mm. The surface of the mixture was ignited with a gas flame under a pressure drop of 500mm H_2O over the bed. The ignition temperature measured on the surface of the sinter bed was 1000°C. After an ignition time of 1.5 minutes the gas flame was stopped and the pressure drop over the sinter bed was increased. **Figure 3** and **Figure 4** are schematic diagrams showing the sinter pot test equipment and set-up. In these tests the pressure drop over the sinter bed was controlled to a nearly constant value. Measurement of the off-gas volumes was done at the outlet of the sinter pot. No correction for volume increase due to water vapour and CO_2 formation was done.

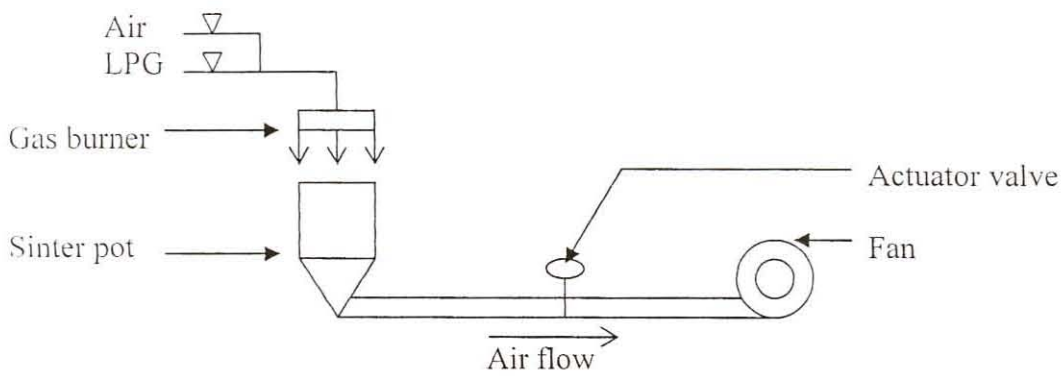

Figure 3: Sinter pot test equipment

In the first series of sinter pot tests the pressure drop was increased to 1100mm H_2O after ignition. The sintering cycle ended when the off-gas temperature reached a maximum temperature and started to decline. In the cooling cycle the sinter was cooled in the sinter pot under a pressure drop of 1100mm H_2O over the sinter bed. The cooling cycle ended when the off-gas temperature reached 150°C. In order to increase the airflow rate through the sinter bed during sintering the pressure drop over the sinter bed was increased to 1500mm H_2O after ignition during the second series of sinter pot tests. The sintering cycle ended when the off-gas temperature reached a maximum temperature and started to decline. In the cooling cycle the sinter was cooled in the sinter pot under a pressure drop of 1500mm H_2O over the sinter bed. The cooling cycle again ended when the off-gas temperature reached 150°C.

Process parameters were recorded during the sinter pot tests in order to characterise the sinter pot test conditions of each series. The temperature profile at different heights in the sinter bed was determined with thermocouples (**Figure 4**) to represent the temperature profile in the top layer, middle layer and bottom layer of the sinter pot. These K-type thermocouples were inserted into the sinter bed before the sinter was ignited by the gas flame.

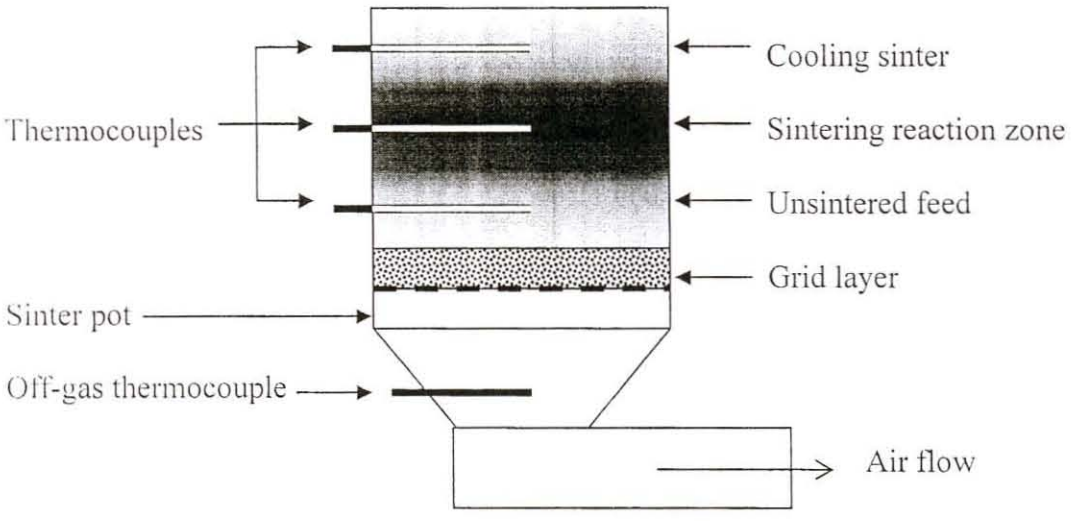

Figure 4: The sinter pot with thermocouples

Three sinter pot tests were performed in each series according to the sinter pot test standard procedure. Each sinter cake obtained from the sinter pot tests was physically divided into three layers to form a top layer, middle layer and bottom layer. The sinter from each layer was combined to produce a representative sample of each layer. The different layers of both series were separately prepared for evaluation. The aim was to characterise the properties of the sinter in the top layer, middle layer and bottom layer of each series.

The sinter was prepared according to a procedure to represent the preparation stage of sinter at the sinter plant. The preparation procedure also ensures that the samples taken from the sinter are representative of the sinter produced in the sinter pot test. Therefore, the different samples represent the sinter in the top layer, the sinter in the middle layer and the sinter in the bottom layer of each series.

A sieve analysis was conducted on each sample. Material representative of the size fraction –40+10mm was prepared for the tumbler test (ISO3271). The tumbler test (ISO3271) was used to determine the physical properties i.e. the strength of the sinter in each sample. Material representative of the size fraction –25+16mm was prepared for chemical and phase analyses.

5. RESULTS AND DISCUSSION

5.1 PRESSURE DROP AND AIRFLOW RATE

In the first series of sinter pot tests the pressure drop over the sinter bed was increased to 1100mm H_2O after the ignition sequence (**Figure 5**). The airflow rate through the sinter bed increased due to the applied pressure drop of 1100mm H_2O (**Figure 6**). During the sintering cycle the permeability of the bed decreased due to the sintering reactions that were taking place and formation of the melt[5]. As a result, the airflow rate decreased to a minimum of 2115 l/minute after 17 minutes. The permeability of the sinter bed improved due to the solidification of the phases resulting in the airflow rate to increase again towards the end of the sintering cycle. The average airflow rate during the sintering cycle was 2983 l/minute.

The sintering cycle ended when the off-gas temperature reached a maximum temperature of 417°C after 21 minutes and started to decline (**Figure 7**). The off-gas temperature increases because the combustion layer moves downwards in the sinter bed and the remaining raw materials mixture does not cool the off-gas any more. The airflow rate at the end of the sintering cycle is almost the same as at the start of the sintering cycle.

In the cooling cycle the sinter was cooled in the sinter pot under a pressure drop of 1100mm H_2O over the sinter bed. The resulting airflow rate is very high due to the microstructure of the sinter which has good permeability. The cooling cycle ended when the off-gas temperature reached 150°C.

Figure 5: Pressure drop during the sinter pot tests

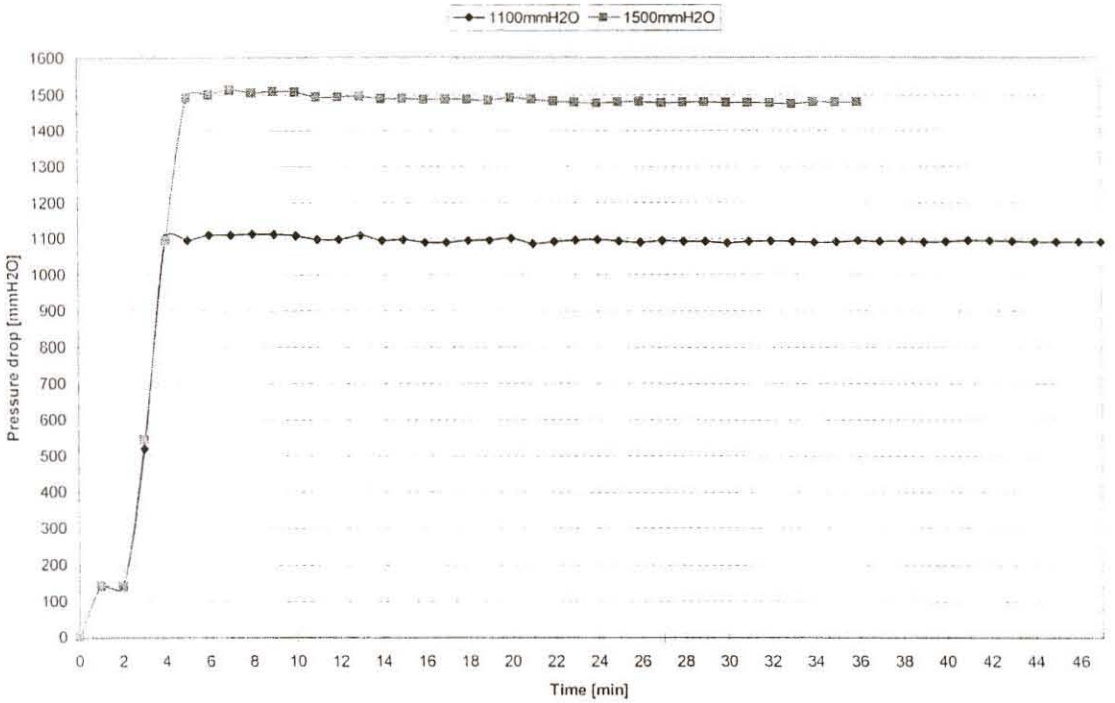

Figure 6: Air flow rate during the sinter pot tests

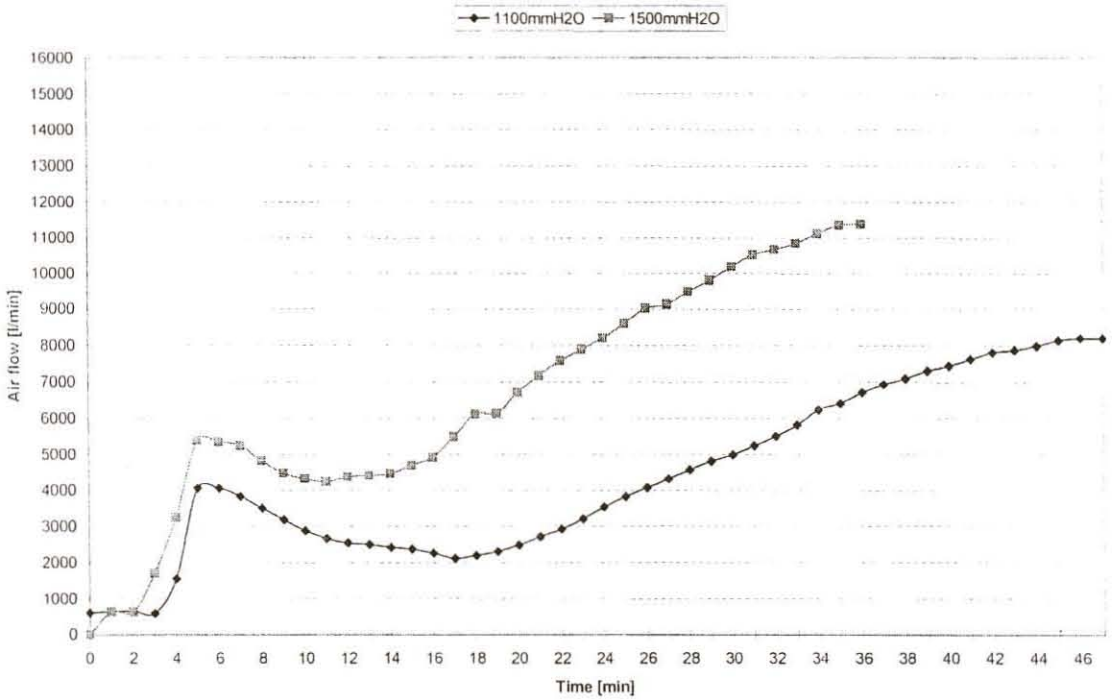

Figure 7: Off-gas temperature during the sinter pot tests

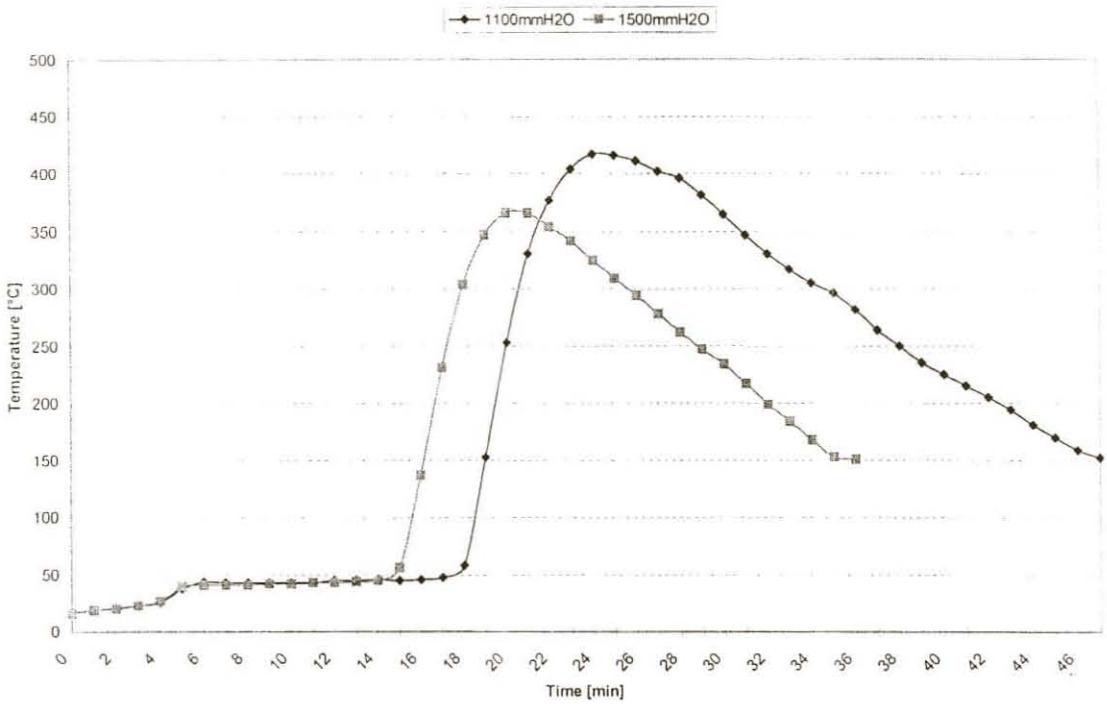

In order to increase the airflow rate through the sinter bed during sintering the pressure drop over the sinter bed was increased to 1500mm H_2O during the second series of sinter pot tests (**Figure 5**). **Figure 6** shows the resulting airflow rate. The airflow rate through the sinter bed increased due to the applied pressure drop of 1500mm H_2O (**Figure 6**). During the sintering cycle the permeability of the bed decreased due to the sintering reactions that were taking place and formation of the melt. As a result, the airflow rate decreased to a minimum of 4237 l/minute after 11 minutes. The permeability of the sinter bed improved due to the formation of sinter resulting in the airflow rate to increase again towards the end of the sintering cycle.

The sintering cycle ended when the off-gas temperature reached a maximum temperature of 366°C after 16 minutes and started to decline (**Figure 7**). The off-gas temperature increases because the combustion layer moves downwards in the sinter bed and the remaining raw materials mixture does not cool the off-gas any more. The airflow rate at the end of the sintering cycle is almost the same as at the start of the sintering cycle.

It is important to note that the airflow rate in the sintering and cooling cycle of series two (1500mm H_2O) was higher than the airflow rate in series one (1100mm H_2O). The increased pressure drop over the sinter bed in series two resulted in the faster downward movement of the reaction zone and therefore a shorter sintering time. Therefore, it is possible to increase the airflow rate and to decrease the sintering time by increasing the pressure drop over the sinter bed. Some of the more important results of both series are summarised in **Table 3**.

Table 3: Pressure drop and airflow rate characteristics of sintering and cooling cycle during Series 1 and Series 2

		Series 1	Series 2
Sintering cycle			
Pressure drop over sinter bed	mmH_2O	1100	1500
Airflow after ignition sequence	l/minute	4062	5389
Minimum airflow	l/minute	2115	4237
Airflow at end of sintering cycle	l/minute	4069	7174
Average airflow rate	l/minute	2983	5194
Duration of sintering cycle	minutes	21	16
Maximum off-gas temperature	°C	417	366
Cooling cycle			
Pressure drop over sinter bed	mmH_2O	1100	1500
Average airflow rate	l/minute	6629	9723
Duration of cooling cycle	minutes	21	15

5.2 TEMPERATURE-TIME-CHARACTERISTICS

The temperature profile at different heights in the sinter bed was determined with thermocouples to represent the temperature profile in the top layer, middle layer and bottom layer of the sinter pot. The temperature profile at 1100mm H_2O is shown in **Figure 8** while the temperature profile at 1500mm H_2O is shown in **Figure 9**.

The temperature-time-characteristics in each layer are summarised in **Table 4**. Heating rates were determined from a straight line tangential to the temperature curve at 700°C. The heating rates in series two with the higher pressure drop over the sinter bed (1500mm H_2O) exceeded the heating rates of series one with the lower pressure drop over the sinter bed (1100mm H_2O).

Figure 8: Temperature profile at 1100mmH_2O

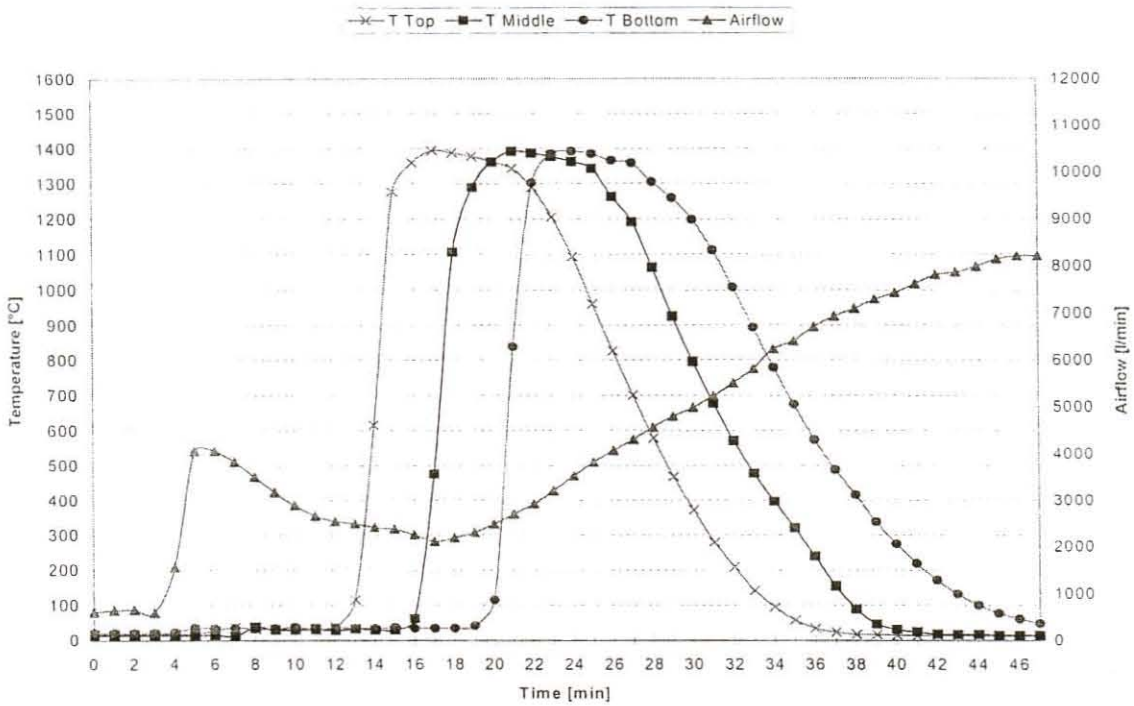

Figure 9: Temperature profile at 1500mmH_2O

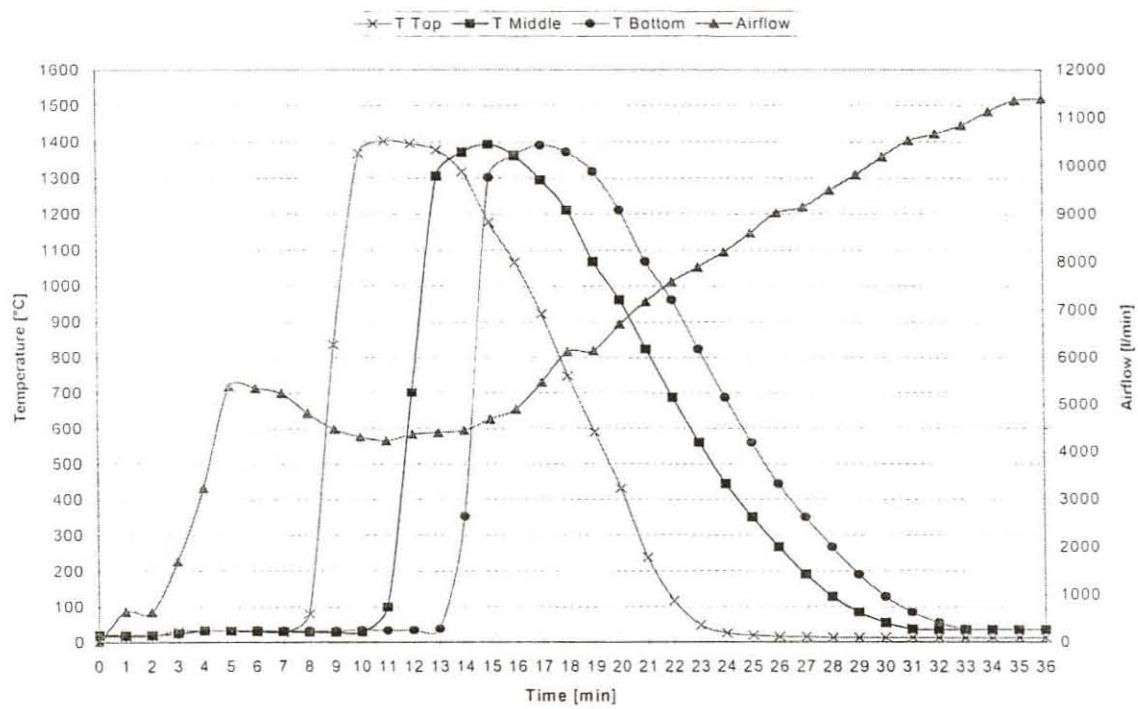

The highest heating rate in both series was found to be in the bottom layer. Reported heating rates are between 700°C/min and 1000°C/min [13]. The maximum temperatures reached in each layer in both series did not differ as much. This is possibly due to the high coke consumption during the sinter pot tests in both series.

Table 4: Temperature-time-characteristics

Parameter	Top	Middle	Bottom
Series 1: 1100mm H_2O			
Heating rate [°C/min]	641	641	751.9
T maximum [°C]	1393	1391	1391
Cooling rate [°C/min]	125	112.5	102.2
Time at T>1100°C [min]	9.3	9.8	9.6
Series 2: 1500mm H_2O			
Heating rate [°C/min]	751.9	641	1123.6
T maximum [°C]	1402	1393	1391
Cooling rate [°C/min]	155.3	132.3	128.5
Time at T>1100°C [min]	6.3	6.4	6.2

Cooling rates were determined from a straight line tangential to the temperature curve at 700°C. Cooling rates in series two were higher than the cooling rate in series one. In both series one and two the highest cooling rate was found to be in the top layer and the lowest cooling rate was found to be in the bottom layer (**Table 4**). Reported cooling rates vary between 100°C/min and 300°C/min [13].

Together with the differences in heating and cooling rates, another important observation is that of the different residence times above 1100°C for each layer. In both series the longest residence time above 1100°C was found to be in the middle layer, while the shortest residence time above 1100°C was found to be in the top layer. The time at temperatures higher then 1100°C for series one (1100mm H_2O) exceeded the time at temperatures higher than 1100°C for series two (1500mm H_2O). The faster downward movement of the reaction layer through the sinter bed resulted in shorter residence times above 1100°C in series two. The residence time above 1100°C is considered as very important because phase formation occurs in this temperature region[4]. It is assumed that the sintering process is complete when the temperature

drops below 1100°C[4]. Therefore, the longer the residence time in this temperature region the more time there will be for phase formation. This may result in the formation of a higher content of phases that will enhance the sinter quality for example SFCA.

The airflow rate through the sinter bed is changed by changing the pressure drop over the sinter bed. The change in airflow rate through the sinter bed effects the rate of the downward movement of the combustion layer. This results in changes in the temperature-time-characteristics as described above during the sintering process.

5.3 PHYSICAL PROPERTIES

The physical properties of the sinter are characterised by the sieve analyses and the resistance to degradation by impact and abrasion at room temperature as determined with the ISO 3271 tumbler strength test. Results are shown in **APPENDIX A**.

The tumbler index (TI) is a relative measure of the resistance of the sinter to breakage by impact and abrasion. The tumbler index is expressed as the percentage of the +6.30mm fraction remaining after the tumbler test. A tumbler index greater than 70% is considered as an acceptable index for sinter. At a tumbler index greater than 70% the size degradation of the sinter by means of breakage by impact and abrasion is low and few fines will be generated.

The abrasion index (AI) is a relative measure of the size degradation of the sinter by means of abrasion. The abrasion index is expressed as the percentage of the -0.5mm fraction present after the tumbler test. An abrasion index smaller than 5% is considered as an acceptable index for sinter. At an abrasion index smaller than 5% the size degradation of the sinter by means of abrasion is low and few fines will be generated.

The results of the tumbler strength test are shown in **Table 5**. The abrasion index (AI) of the sinter in all the layers in both series is below 5% and is considered as an acceptable index for the sinter produced in these sinter pot tests. The results of the

tumbler test indicate that there is not a big difference between the physical properties of the sinter in the two different series (**Figure 10**). However, the results of the tumbler test imply that the physical properties of the sinter improved from the top layer to the bottom layer. Also note that the tumbler index of the sinter in the bottom layer of series one is lower than the tumbler index of the sinter in the bottom layer of series two.

Table 5: Tumbler and abrasion index of sinter produced in each layer

Parameter	Top	Middle	Bottom
Series 1: 1100mm H_2O			
TI (%+6.30mm)	46.12	61.39	68.80
TI (%-6.30+0.50mm)	49.89	34.00	26.50
AI (%-0.50mm)	3.99	4.61	4.70
Series 2: 1500mm H_2O			
TI (%+6.30mm)	42.80	60.60	72.10
TI (%-6.30+0.50mm)	53.30	35.10	23.30
AI (%-0.50mm)	3.90	4.30	4.60

Figure 10: Tumbler index of sinter produced in each layer

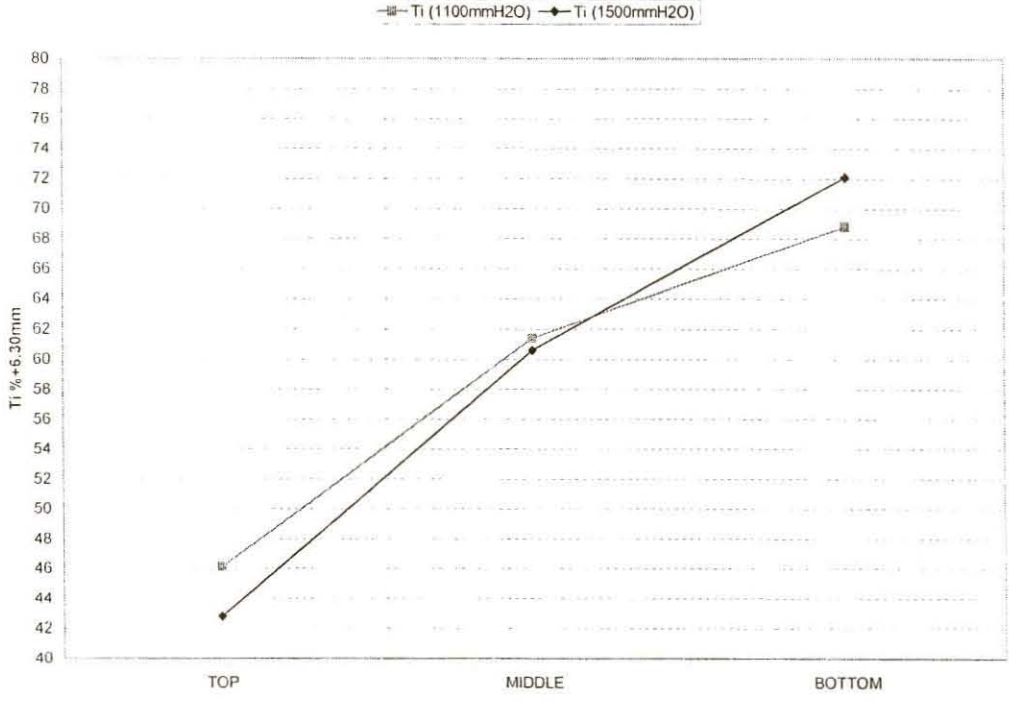

The results of the sieve analysis together with two important size fractions are shown in **Table 6** and are evaluated in conjunction with the tumbler index.

Table 6: Sieve analysis

Particle size	Series1: 1100mmH_2O			Series 2: 1500mmH_2O		
mm	Top	Middle	Bottom	Top	Middle	Bottom
+40	1.40	6.23	14.90	0.00	2.55	5.01
-40+25	4.66	18.97	24.20	3.27	13.00	10.49
-25+16	18.72	27.30	24.53	12.56	29.73	19.15
-16+12.5	13.33	11.98	9.15	12.41	12.90	16.78
-12.5+10	11.60	7.75	6.60	12.52	9.47	11.49
-10+5	32.88	16.49	12.11	39.64	20.92	23.23
-5	17.42	11.27	8.52	19.59	11.43	13.85
Fractions						
+16	24.78	52.50	63.63	15.83	45.28	34.65
-10	50.30	27.76	20.63	59.23	32.35	37.08
Mean size						
mm	13.75	20.25	24.17	11.82	17.57	17.05

More fines (-10mm) are produced in series two than in series one. It is also clear that the quantity of fines decreases from the top layer to the bottom layer. The quantity of the +16mm size material increases from the top layer to the bottom layer. The quantity of the +16mm size material produced in series one is higher than the quantity of the +16mm size material produced in series two (**Table 6**).

The mean particle size of the sinter in series one is also higher than the mean particle size of the sinter in series two (**Table 6**). The mean particle size increases from the top layer to the bottom layer in each series. These results indicate that the physical properties of the sinter in series one are better than the physical properties of the sinter in series two and that the physical properties improved from the top layer to the bottom layer.

Although it is not very clear from the tumbler index, it can be concluded from the sieve analysis that the physical properties of the sinter produced in series one (1100mm H_2O) are better than the physical properties of the sinter produced in series two (1500mm H_2O). The physical properties of the sinter improved from the top layer to the bottom layer as indicated by the tumbler index and sieve analysis.

5.4 STANDARD DEVIATION OF PHYSICAL PROPERTIES

Four additional sinter pot tests were carried out using the test procedure described in this report. The sinter mixture was the same as the mixture used in this project. The physical properties of the sinter produced in each sinter pot test were determined with the tumbler test (ISO 3271). The standard deviation of the results was calculated and is shown in **Table 7**. The results clearly show that the test procedure and results are repeatable.

Table 7: Standard deviation of tumbler index

Tumbler test results	A	B	C	D	Average	Standard deviation
TI %+6.30mm	70.38	71.17	70.74	70.81	70.78	0.32
TI %-6.30+0.50mm	25.06	24.36	24.92	24.93	24.82	0.31
AI %-0.50mm	4.56	4.46	4.34	4.26	4.41	0.13

5.5 PHASE COMPOSITION

Samples from each layer were prepared for chemical analyses (ICP) and the results are shown in **APPENDIX B**.

Samples were taken from each layer ensuring that the samples represent the sinter in that specific layer. Each representative sample was mounted in epoxy resin and then vacuum impregnated. The samples were polished to expose a plane section. After polishing, the samples were examined under an optical microscope. The volume proportions of phases in the sinter were estimated by using the point counting method. Around 1000 points were counted for the whole polished surface of the sample. The standard deviation of the results obtained by this method is ±0.5%. Results are shown in **APPENDIX C**.

With an energy dispersive microanalyser (EDA) attached to the scanning electron microscope (SEM) it was possible to obtain a quantitative analysis of each phase. The results of the quantitative analysis of each phase were used to calculate the

stoichiometry of each phase. Microphotographs were taken to illustrate the phases and their occurrence in the sinter samples.

5.5.1 HEMATITE

Three types of hematite commonly occur in this sinter. Massive hematite particles resemble the original hematite particles added to the raw materials mixture. These particles were only partially affected during sintering. Some of the massive hematite particles display recrystallised outer rims. In all the layers massive hematite dominates as the hematite phase. More than 75% of the hematite consists of massive hematite. An example of the microstructure containing massive hematite is shown in **Figure 11**.

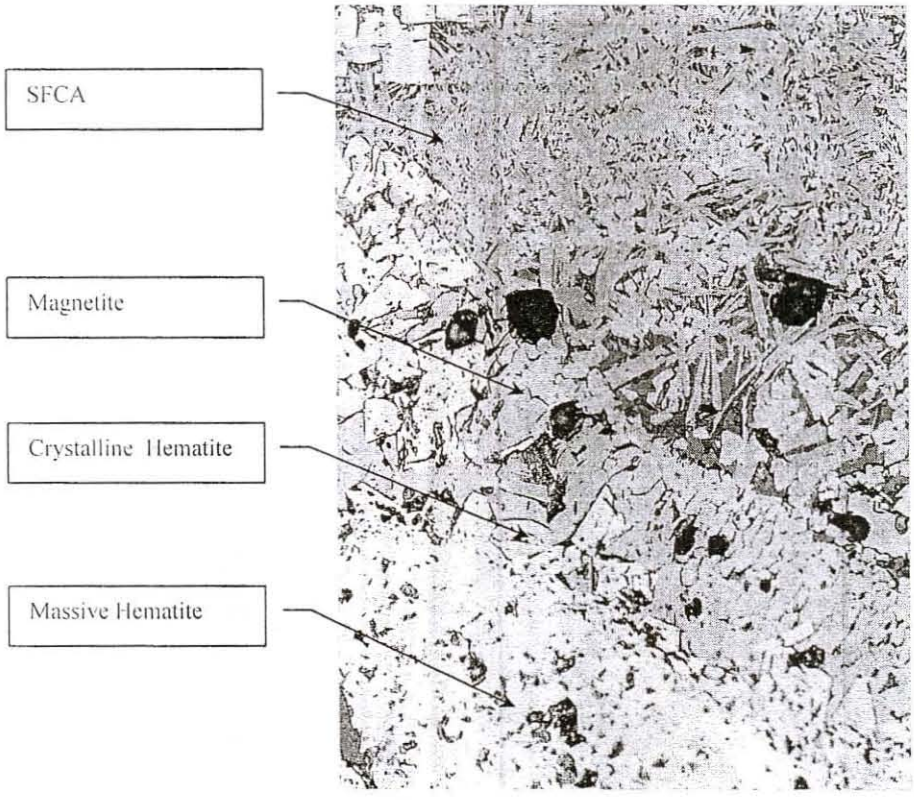

***Figure 11**: Massive hematite displaying a recrystallised rim of crystalline hematite. The hematite is associated with euhedral to subhedral magnetite crystals embedded in a silicate-rich glassy matrix (X 200).*

Magnetite follows the crystalline hematite at the periphery of the massive hematite particles (**Figure 11**). The crystalline hematite occurs as euhedral to subhedral as well

as skeletal and/or dendritic hematite crystals, which crystallise during cooling of the sinter. Approximately 20% of the hematite produced is crystalline hematite that precipitated from the melt.

The remaining hematite consists of very small quantities of secondary hematite. Secondary hematite is in general relatively scarce and probably crystallised due to re-oxidation of magnetite at high temperatures. Secondary hematite is usually bound in a matrix of calcium silicate and SFCA.

The hematite content of the sinter in series one decreased from the top layer to the bottom layer while the hematite content in the sinter in series two reached a maximum in the middle and decreased slightly in the bottom layer (**Figure 12**). The hematite content of series one (1100mmH_2O) is lower than the hematite content of series two (1500mmH_2O). The hematite content correlates with the magnetite content. The higher the magnetite content is, the lower is the hematite content.

Figure 12: Volume percentage of hematite

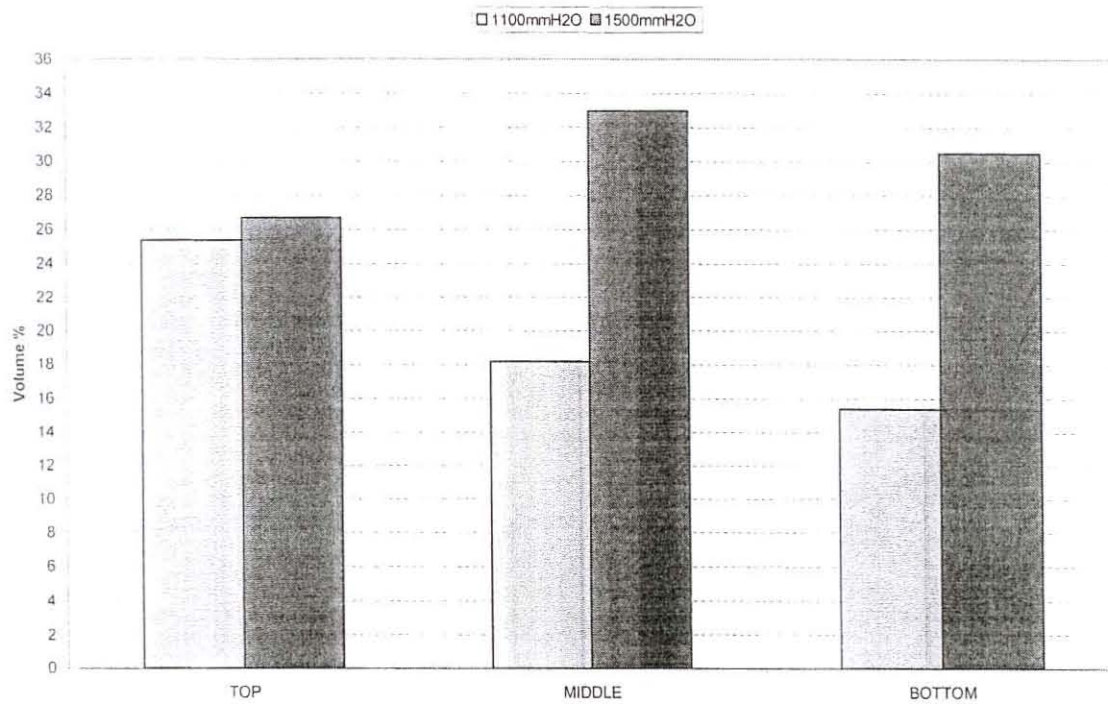

The chemical composition of hematite is shown in **Table 8**. The recalculation to determine the $\%Fe_2O_3$ is shown in **APPENDIX G**. The chemical composition of the hematite present in each layer is almost the same for both series of sinter pot tests as is evident from **Table 8**. A hypothesis test was conducted (**APPENDIX D**) to determine the relation between the chemical composition of the hematite in the different sinter layers. The hypothesis test indicated that there is no difference in the mean Fe_2O_3 content of the different layers.

Table 8: Chemical analyses of hematite

	Series1: 1100mmH_2O			Series 2: 1500mmH_2O		
	Top	**Middle**	**Bottom**	**Top**	**Middle**	**Bottom**
Fe_2O_3	96.81	95.42	96.66	97.03	95.71	95.35
FeO	0.00	0.00	0.00	0.00	0.00	0.00
SiO_2	0.12	0.01	0.07	0.16	0.83	0.37
TiO_2	0.10	0.26	0.18	0.17	0.04	0.09
CaO	0.26	0.30	0.31	0.19	0.71	0.53
SO_3	0.00	0.00	0.00	0.00	0.00	0.00
MnO	0.34	0.12	0.31	0.06	0.12	0.15
K_2O	0.01	0.00	0.00	0.01	0.00	0.00
MgO	0.14	0.01	0.01	0.01	0.07	0.01
Al_2O_3	0.88	1.54	0.59	0.53	0.33	1.07
Na_2O	0.01	0.00	0.01	0.00	0.01	0.00
P_2O_5	0.00	0.00	0.00	0.02	0.01	0.01

5.5.2 MAGNETITE

Magnetite could form during crystallisation from the melt or solid state reduction of hematite or solid state oxidation of wustite[13]. The magnetite is present as well defined euhedral to sub-hedral crystals as well as skeletal and dendritic crystals. Magnetite crystals are present in close association with SFCA, as shown in **Figure 13**.

The magnetite content in the middle and bottom layer of series one is higher than the magnetite content in the middle and bottom layer of series two (**Figure 14**). There is not a significant difference between the magnetite content in the top layers of both series.

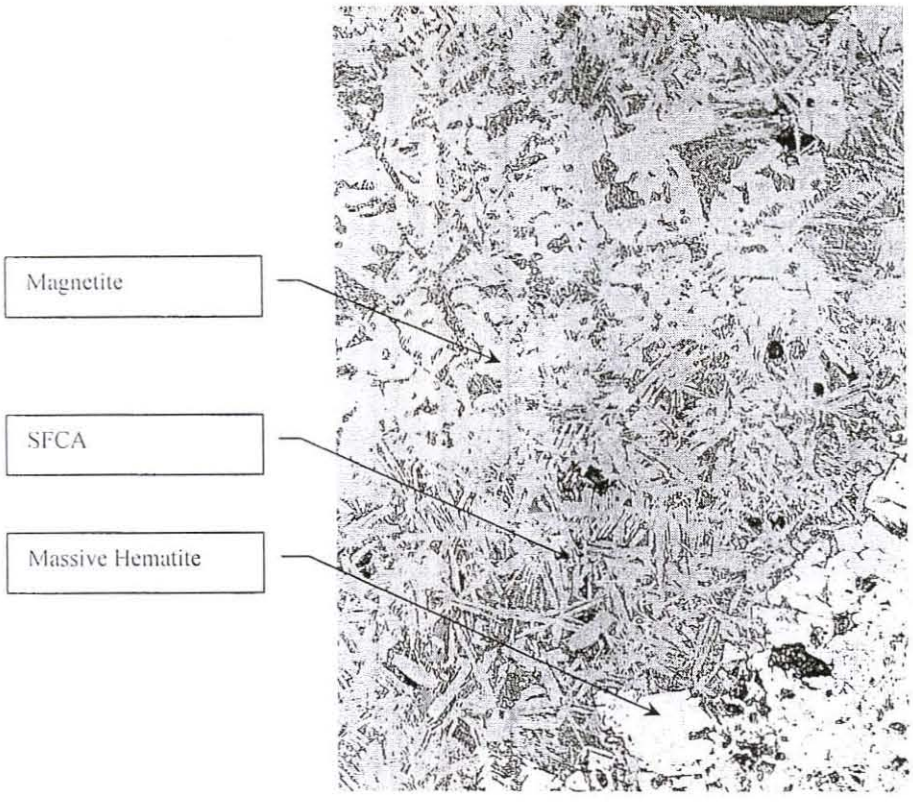

Figure 13: Magnetite crystals embedded in a silicate-rich glassy matrix. The magnetite is in close association with SFCA crystals (X 200).

Figure 14: Volume percentage of magnetite

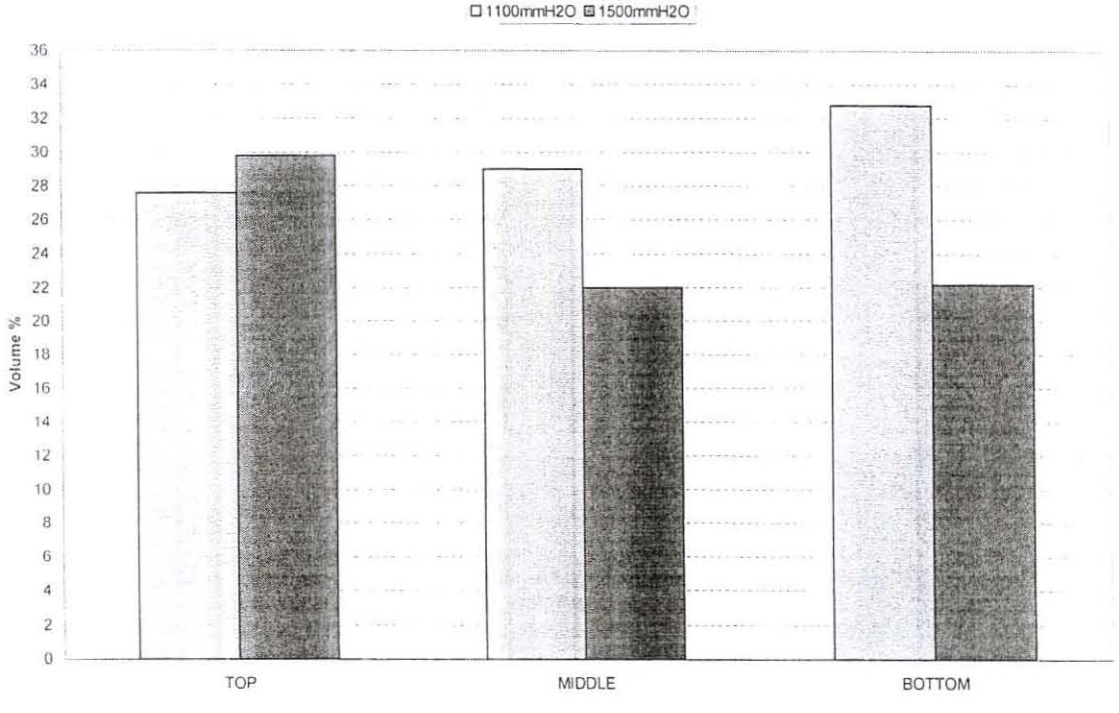

At a low airflow rate the sintering time at temperatures above 1100°C is longer. During sintering the surface of the hematite particle is reduced to magnetite. Due to the longer reaction time, more hematite is reduced to magnetite in series one than in series two.

Magnetite is also formed from the dissociation of SFCA at temperatures higher than 1300°C[(2)(4)]. The proportion of SFCA that is decomposed may increase when the time of exposure above the decomposition temperature increases or when the maximum temperature that is reached during sintering increases. Due to the longer time above 1300°C more magnetite was formed in series one than in series two.

The chemical composition of magnetite is shown in **Table 9**. The recalculation to determine the $\%Fe_2O_3$ and %FeO is shown in **APPENDIX G**. The chemical composition (**Table 9**) of the magnetite in the different layers is almost the same in both series of sinter pot tests.

Table 9: Chemical analyses of the magnetite

	Series1: 1100mmH_2O			Series 2: 1500mmH_2O		
	Top	**Middle**	**Bottom**	**Top**	**Middle**	**Bottom**
Fe_2O_3	69.20	67.71	69.31	67.59	68.06	68.51
FeO	19.10	21.57	20.35	23.29	19.83	19.11
SiO_2	0.02	0.08	0.05	0.12	0.10	0.03
TiO_2	0.01	0.04	0.02	0.04	0.02	0.02
CaO	2.07	1.86	2.04	2.39	2.11	2.42
SO_3	0.00	0.00	0.00	0.00	0.00	0.00
MnO	1.73	1.48	1.86	1.16	2.73	1.72
K_2O	0.00	0.00	0.00	0.00	0.00	0.00
MgO	4.74	3.50	4.08	2.37	3.56	4.42
Al_2O_3	1.22	1.54	1.27	1.58	1.21	1.44
Na_2O	0.00	0.00	0.01	0.00	0.01	0.01
P_2O_5	0.00	0.00	0.00	0.01	0.01	0.00

Figure 15 and **Figure 16** shows the mass percentage (Fe_2O_3 + Al_2O_3) versus the mass percentage (FeO + MgO + CaO + MnO). The well-grouped data as shown by **Figure 15** and **Figure 16** indicate that the chemical composition of the magnetite in the different layers is almost the same. A hypothesis test was conducted (**APPENDIX E**) to determine the relation between the chemical composition of the magnetite in the

different sinter layers. The hypothesis test indicated that there is no difference in the chemical composition of the different layers.

Figure 15: Magnetite (Series 1)

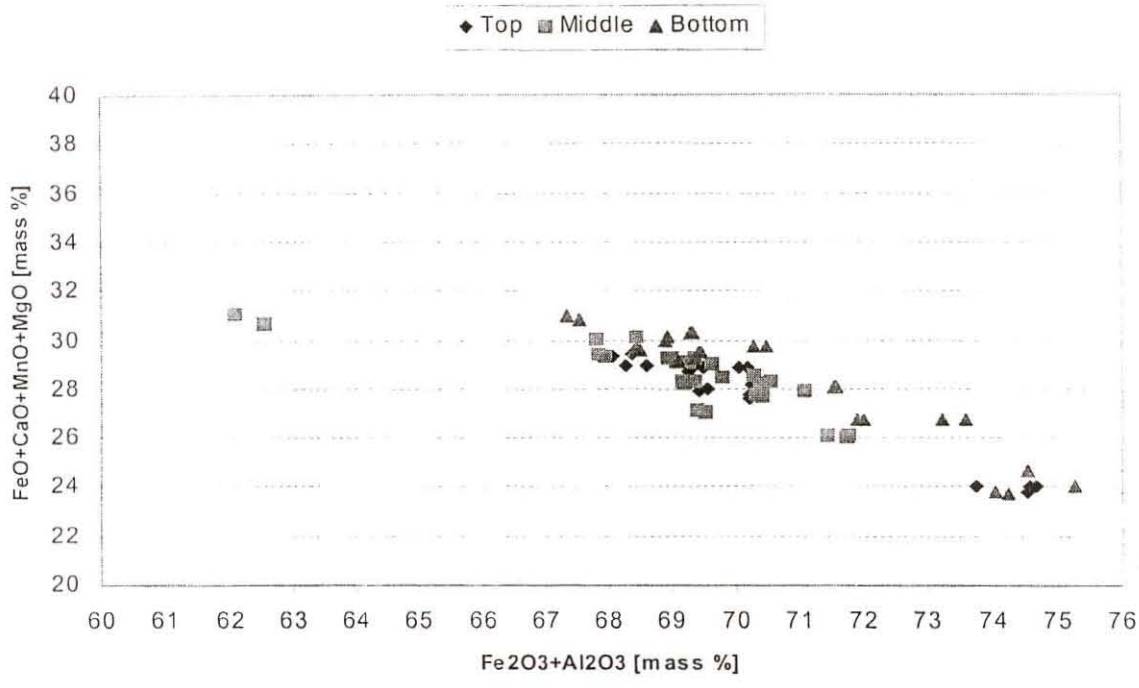

Figure 16: Magnetite (Series 2)

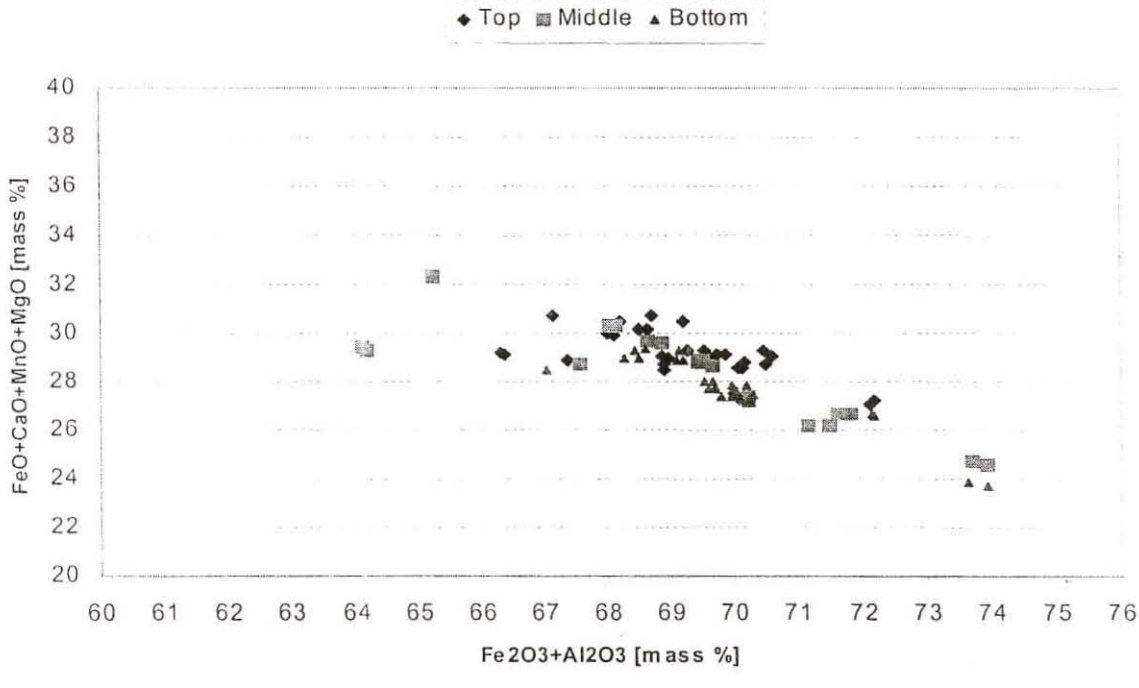

The calculated stoichiometry (**Table 10**) of the magnetite in all the layers agrees very well with the generally accepted formula for magnetite. The generally accepted formula for magnetite is XY_2O_4 = $(Fe,Mg,Si,Ca,Mn)(Fe,Al)_2O_4$. An example to show how the stoichiometry was calculated is shown in **APPENDIX G**.

Table 10: Stoichiometry of the magnetite

XY_2O_4 = $(Fe,Mg,Si,Ca,Mn)(Fe,Al)_2O_4$

	Series1: 1100mmH_2O			Series 2: 1500mmH_2O		
	Top	**Middle**	**Bottom**	**Top**	**Middle**	**Bottom**
Fe^{2+}	0.60	0.68	0.64	0.74	0.63	0.60
Mg^{2+}	0.26	0.20	0.22	0.13	0.20	0.25
Si^{4+}	0.00	0.00	0.00	0.00	0.00	0.00
Ca^{2+}	0.08	0.07	0.08	0.10	0.08	0.10
Mn^{2+}	0.05	0.05	0.06	0.04	0.09	0.05
X	**1.00**	**1.01**	**1.00**	**1.01**	**1.01**	**1.00**
Fe^{3+}	1.95	1.92	1.94	1.92	1.94	1.93
Al^{3+}	0.05	0.07	0.06	0.07	0.05	0.06
Y	**2.00**	**1.99**	**2.00**	**1.99**	**1.99**	**2.00**
O^{2-}	**4.00**	**4.00**	**4.00**	**4.00**	**4.00**	**4.00**

5.5.3 SFCA

SFCA usually contains SiO_2 and Al_2O_3 and is referred to as silico-ferrites of calcium and aluminium (SFCA). SFCA are present as dendritic SFCA, acicular SFCA and tabular SFCA according to the size of the crystals.

Dendritic SFCA is the first type of SFCA formed during the sintering process[9]. Dendritic crystals are very small, usually smaller than 4μm (**Figure 17**). Approximately 15% of the total SFCA consist of dendritic SFCA.

Crystal growth between 1200°C and 1300°C results in bigger crystals, bigger than 4μm but smaller than 10μm, called acicular SFCA[9] as shown in **Figure 18**. Acicular SFCA dominates as the SFCA phase in all the layers. More than 75% of the total SFCA consists of acicular SFCA.

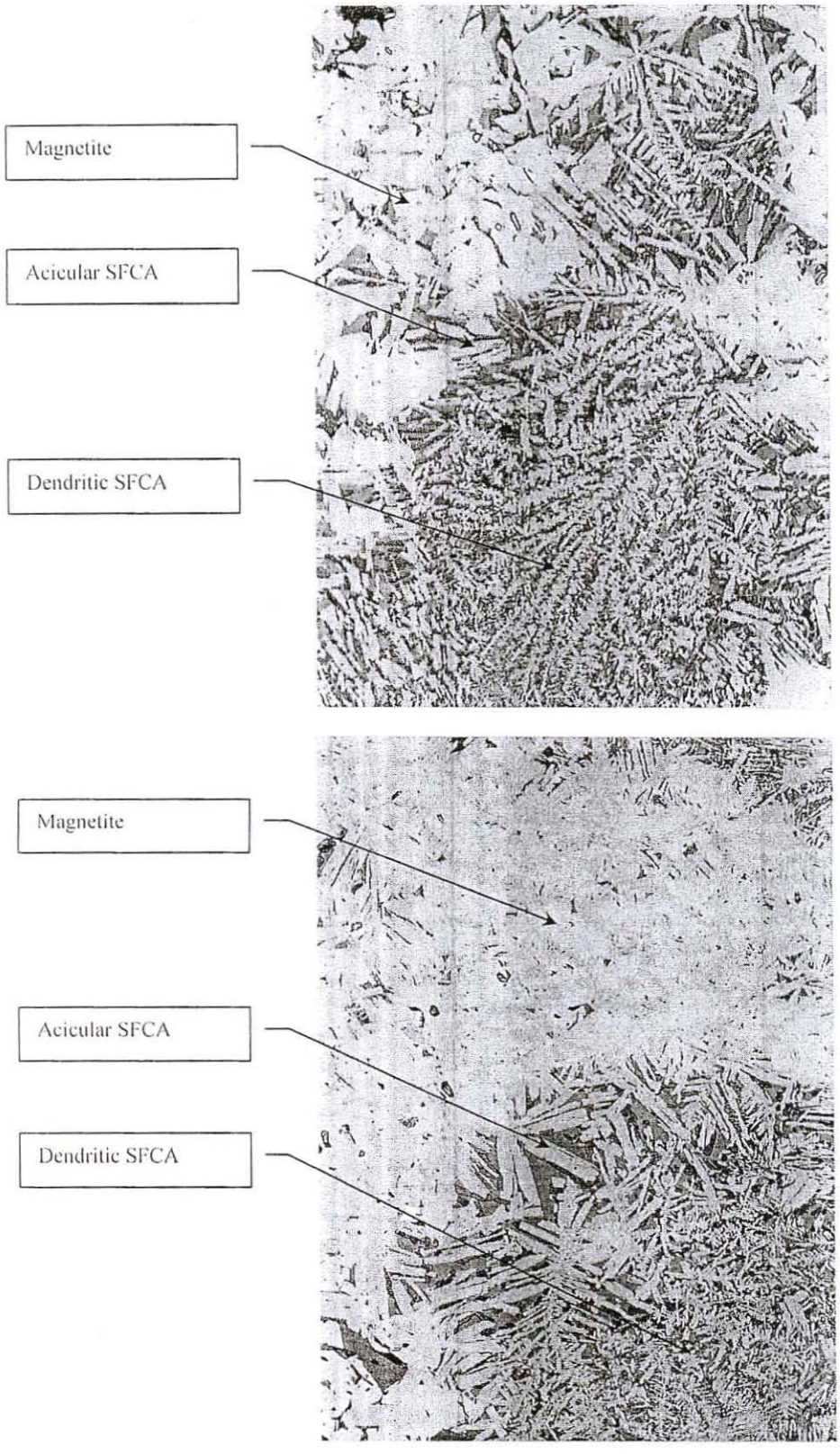

***Figures 17 and 18**: Dendritic SFCA is the first type of SFCA formed during the sintering process. Crystal growth results in bigger crystals called acicular SFCA (X 200).*

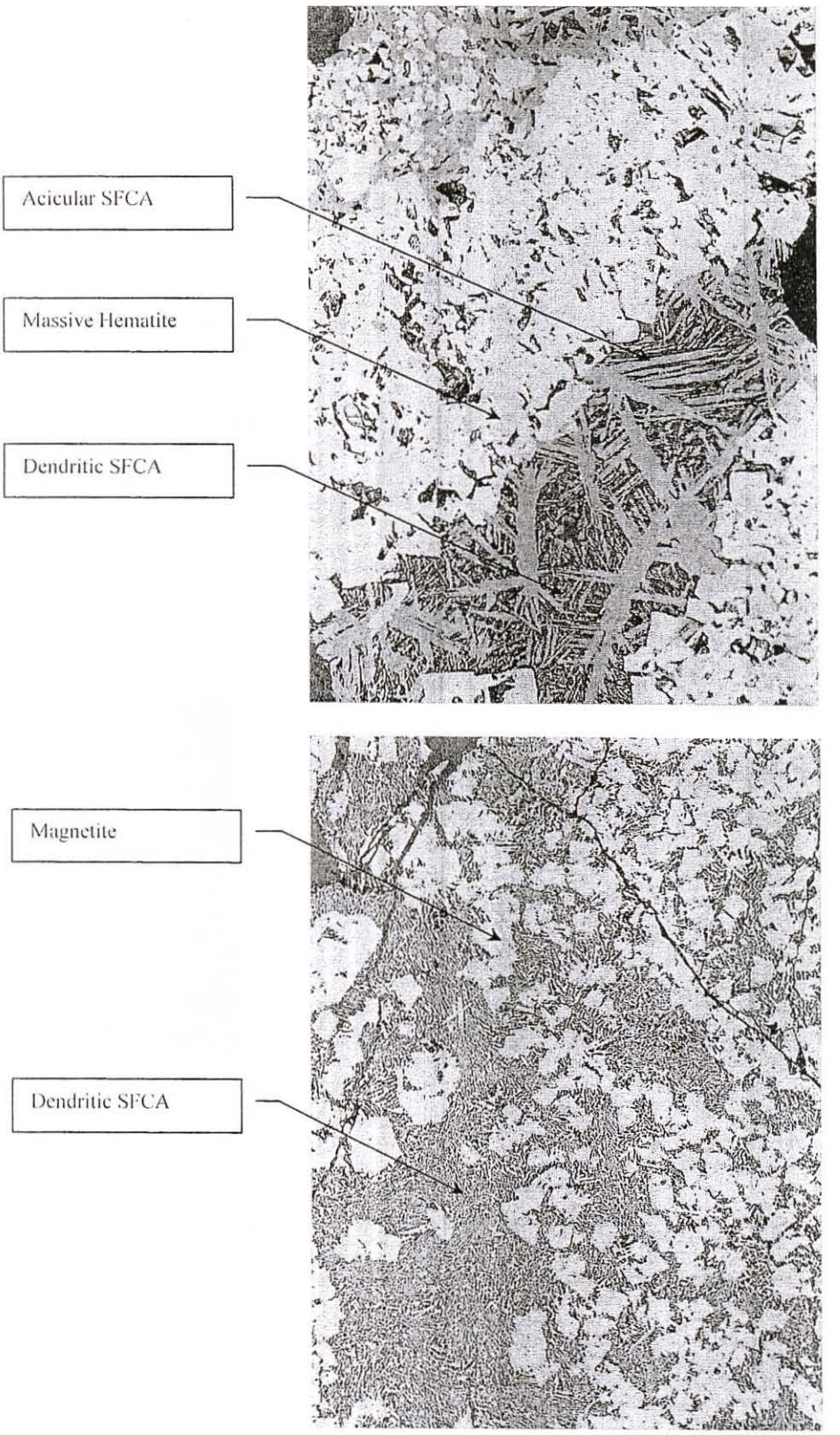

***Figures 19 and 20**: SFCA in association with massive hematite and SFCA in association with magnetite (X 200).*

At 1300°C acicular SFCA melts and precipitates as columnar SFCA during cooling. These are rather large crystals with a typical size of 10μm and bigger[9]. Approximately 10% of the total SFCA consist of columnar SFCA.

In series one the highest SFCA content is found to be in the middle layer and the lowest in the top layer. In series two the total SFCA content increased from the top layer to the bottom layer (**Figure 21**). The total SFCA content of series one is higher than the total SFCA content of series two.

Figure 21: Volume percentage of SFCA

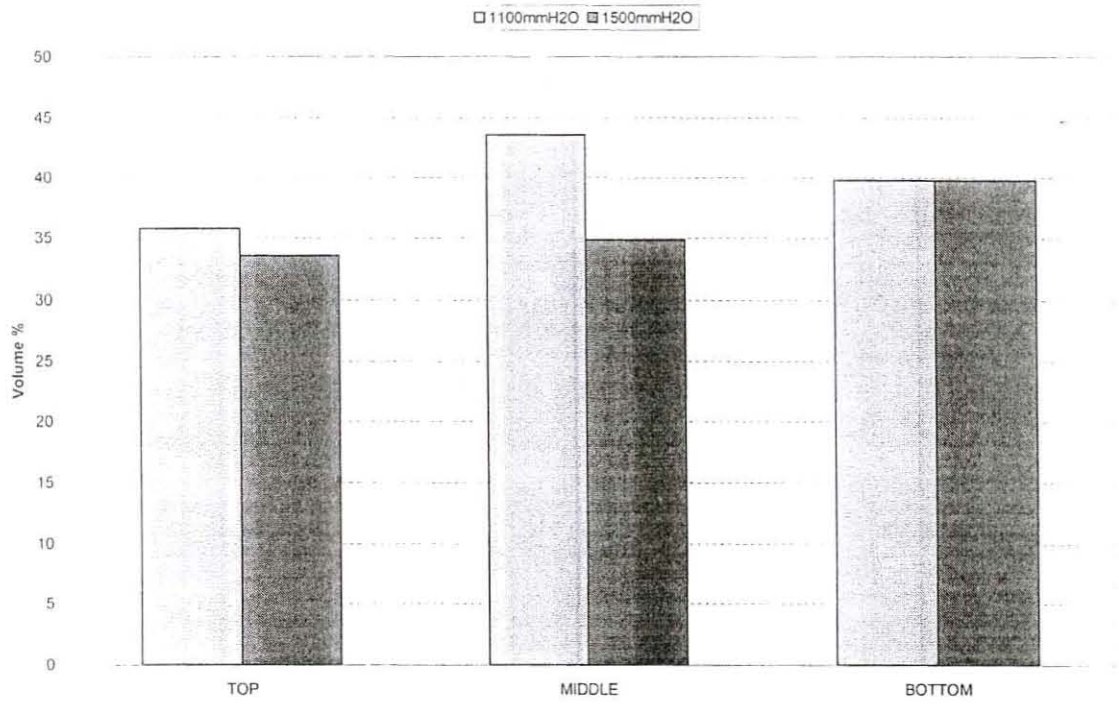

SFCA is the product of several successive reactions[14]:

1. The formation of monocalcium ferrite at temperatures from 1050°C to 1150°C.
2. The reaction between Al_2O_3 and CaO to produce calcium aluminate (1100°C-1150°C).
3. Dissolution of the calcium aluminate in monocalcium ferrite at 1100°C-1150°C to produce aluminous monocalcium ferrite.
4. Fusion of the aluminous monocalcium ferrite and reaction with Fe_2O_3 at 1200°C-1250°C to produce aluminous hemicalcium ferrite.
5. Reaction with SiO_2 at 1200°C-1250°C to produce SFCA.

From the above it is clear that the formation of SFCA will be enhanced by a longer time at temperatures above 1100°C. At a low airflow rate the sintering time at temperatures above 1100°C is longer. Therefore, the higher SFCA content in series one. The sintering time at temperatures above 1100°C increased from the top layer to the bottom layer resulting in a higher SFCA content in the middle and bottom layers.

The SFCA will begin to decompose when the temperature exceeds 1300°C[2][4]. At decomposition it will change to hematite when the partial pressure of oxygen is high and the temperature is lower than 1350°C. It will change to magnetite when the partial pressure of oxygen is low and the temperature is higher than 1350°C[2]. The proportion of SFCA that is decomposed may increase when the time of exposure above the decomposition temperature increases or when the maximum temperature that is reached during sintering increases. Therefore, it is important to control the maximum sintering temperature below 1300°C to prevent decomposition of SFCA.

The chemical composition of SFCA is shown in **Table 11**. The recalculation to determine the $\%Fe_2O_3$ and %FeO is shown in **APPENDIX G**. The chemical composition (**Table 11**) of the SFCA in the different layers is almost the same in both series of sinter pot tests.

Table 11: Chemical analyses of SFCA

	Series1: 1100mmH_2O			**Series 2: 1500mmH_2O**		
	Top	**Middle**	**Bottom**	**Top**	**Middle**	**Bottom**
Fe_2O_3	75.89	73.42	73.95	77.10	77.03	78.58
FeO	0.00	0.00	0.00	0.00	0.00	0.00
SiO_2	6.01	6.63	6.44	5.04	4.94	4.69
TiO_2	0.22	0.16	0.21	0.14	0.13	0.12
CaO	14.98	14.72	14.57	14.05	13.23	12.61
SO_3	0.00	0.00	0.00	0.02	0.00	0.02
MnO	0.56	0.51	0.72	0.58	1.36	0.89
K_2O	0.01	0.00	0.00	0.03	0.00	0.02
MgO	1.06	0.80	0.87	0.83	1.02	1.88
Al_2O_3	3.46	4.16	4.88	3.99	3.95	3.60
Na_2O	0.01	0.01	0.01	0.02	0.01	0.02
P_2O_5	0.02	0.00	0.01	0.19	0.02	0.03

Figure 22: SFCA (Series 1)

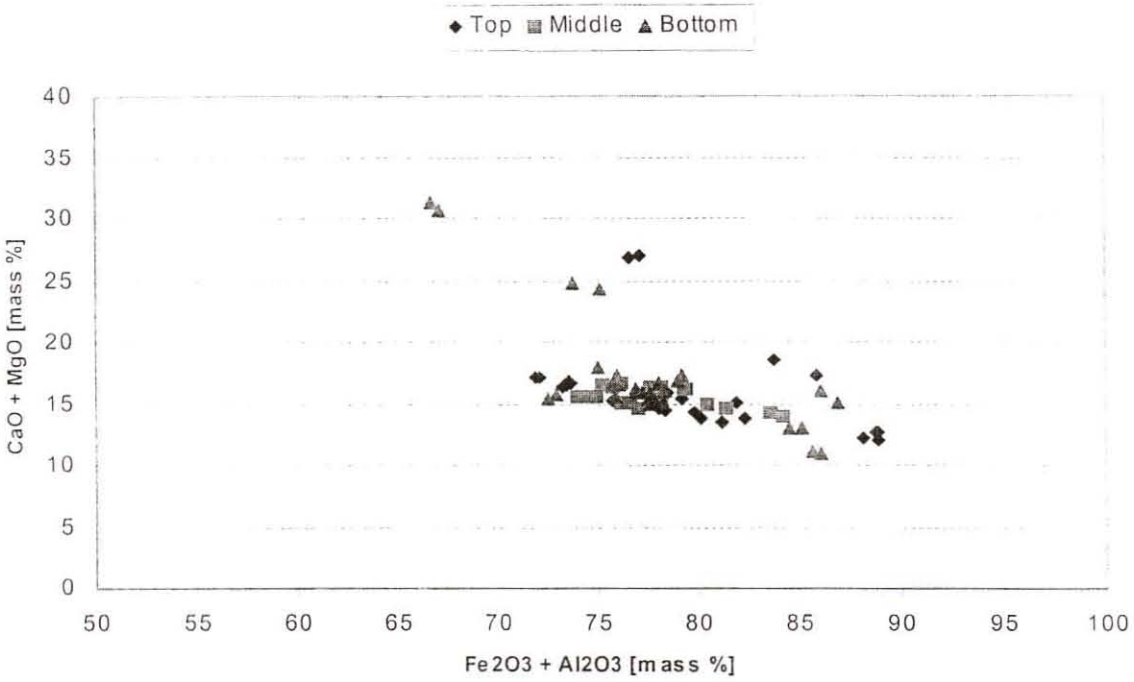

Figure 23: SFCA (Series 2)

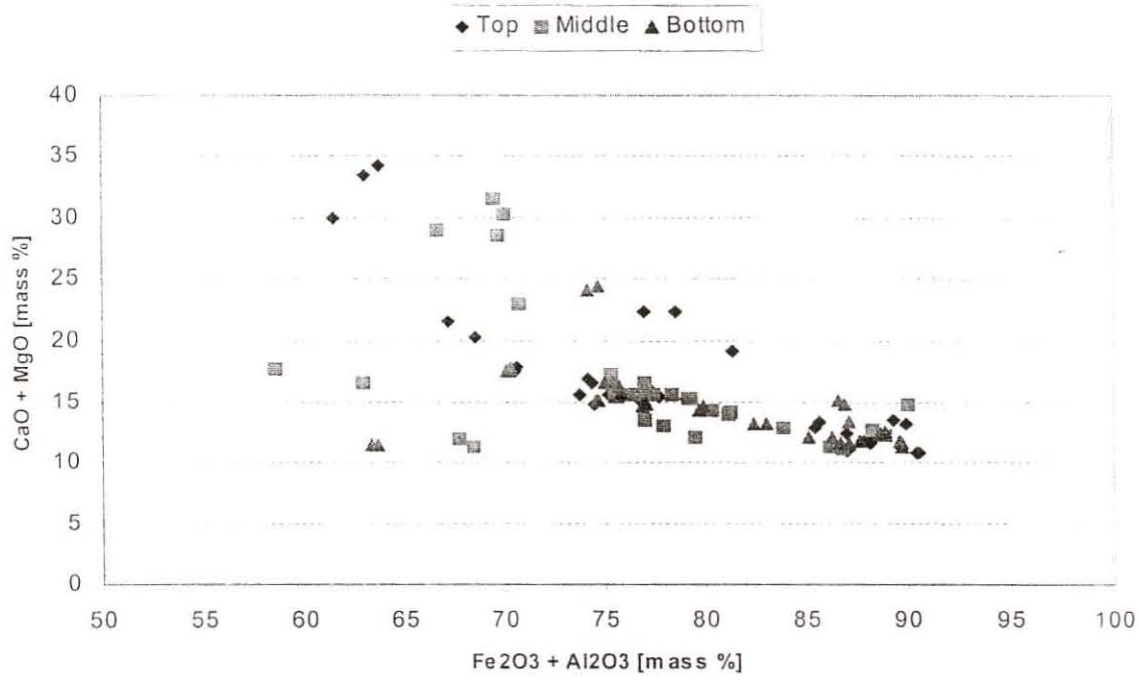

Figure 22 and **Figure 23** show the mass percentage (Fe_2O_3 + Al_2O_3) versus the mass percentage (CaO + MgO). The hypothesis tests (**APPENDIX F**) and well grouped data as shown in **Figure 22** and **Figure 23** indicates that the chemical composition of the SFCA in the different layers is almost the same. However, a few samples in series two were scattered due to the SiO_2 content higher than 10%. The most common empirical formula for SFCA is $M_{25}O_{36}$ [13]. The calculated stoichiometry (**Table 12**) of the SFCA in all the layers agrees well with the general formula $M_{25}O_{36}$ = $Ca_5,Si_2,(Fe,Al)_{18}O_{36}$. An example to show how the stoichiometry was calculated is shown in **APPENDIX G**.

Table 12: Stoichiometry of SFCA

$M_{25}O_{36} = Ca_5,Si_2,(Fe,Al)_{18}O_{36}$

	Series1: 1100mmH_2O			Series 2: 1500mmH_2O		
	Top	**Middle**	**Bottom**	**Top**	**Middle**	**Bottom**
Ca^{2+}	4.82	4.74	4.63	4.56	4.31	4.08
Si^{4+}	1.80	1.99	1.90	1.51	1.49	1.41
Fe^{3+}	17.17	16.55	16.50	17.57	17.61	17.90
Al^{3+}	1.23	1.47	1.70	1.41	1.40	1.28
M	**25.02**	**24.75**	**24.73**	**25.05**	**24.81**	**24.67**
O^{2-}	**36.00**	**36.00**	**36.00**	**36.00**	**36.00**	**36.00**

5.5.4 OTHER PHASES

The sinter contained an amorphous silicate rich glass. In some instances the glass appeared to be finely crystalline with lath like olivine crystals crystallising from the glass upon cooling of the melt.

Wustite / magnesiowustite is only present in small quantities and occurs as fine to medium grained spherical particles. The periclase is mainly present as grainy type aggregate particles consisting of abundant fine grained spherical MgO crystals and particles as shown in **Figure 25**. MnO-rich (Mn,Fe,Mg)O particles were optically observed (**Figure 24**) in some of the sinter samples. Optically this phase resembles magnetite but the individual oxide crystals display well defined twinning with strong anisotropic texture that is absent in magnetite.

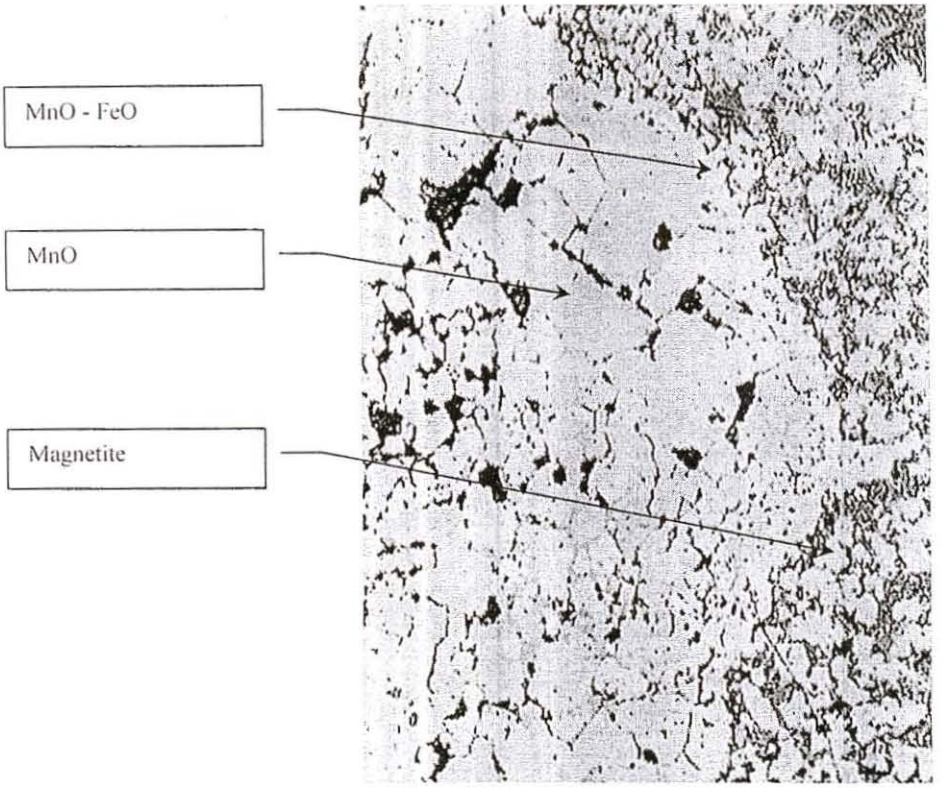

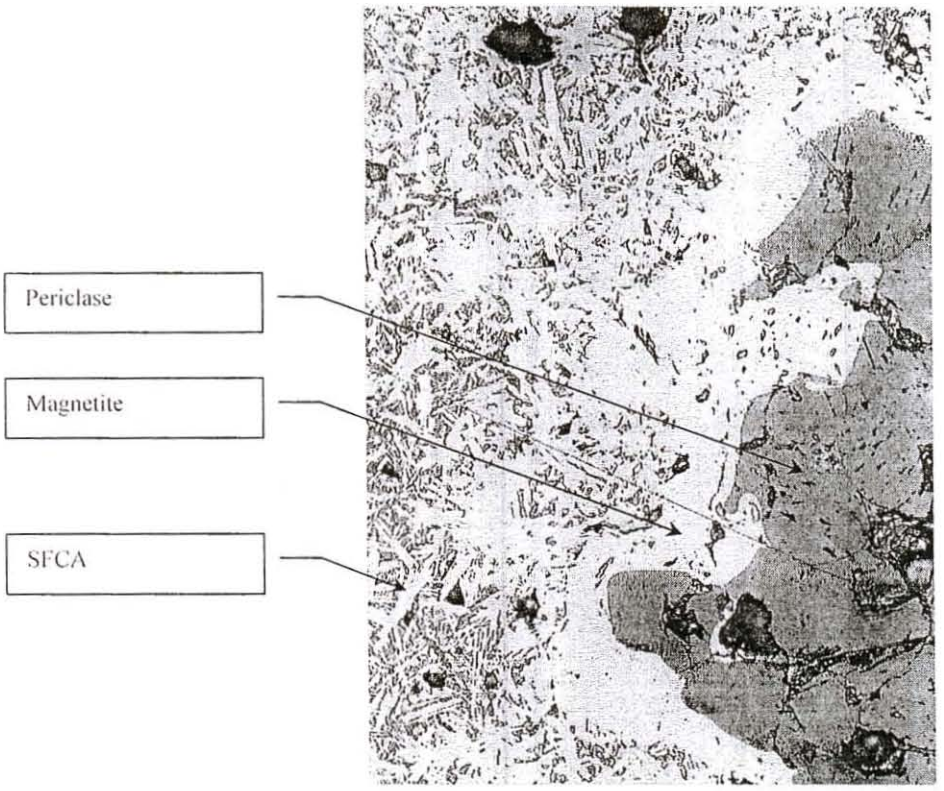

***Figures 24 and 25**: Other phases present in the sinter include manganese oxide and periclase (X 200).*

Small quantities of calcium silicate, glass, periclase, wustite and manganese occur in the sinter (**Figure 26 and 27**).

Figure 26: Other phases (Series 1)

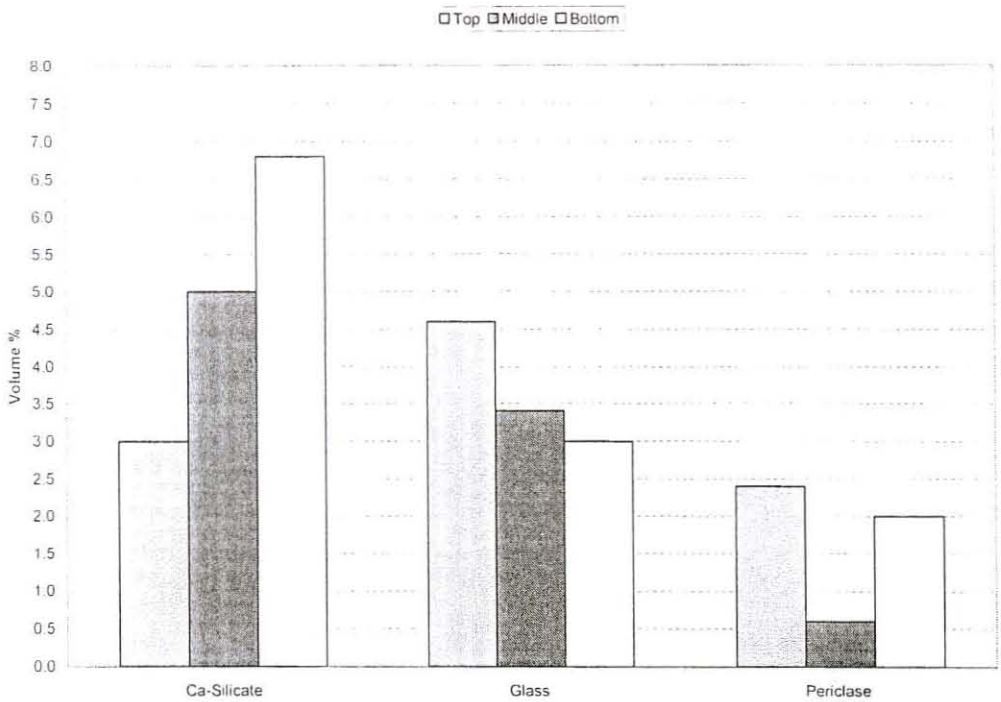

Figure 27: Other phases (Series 2)

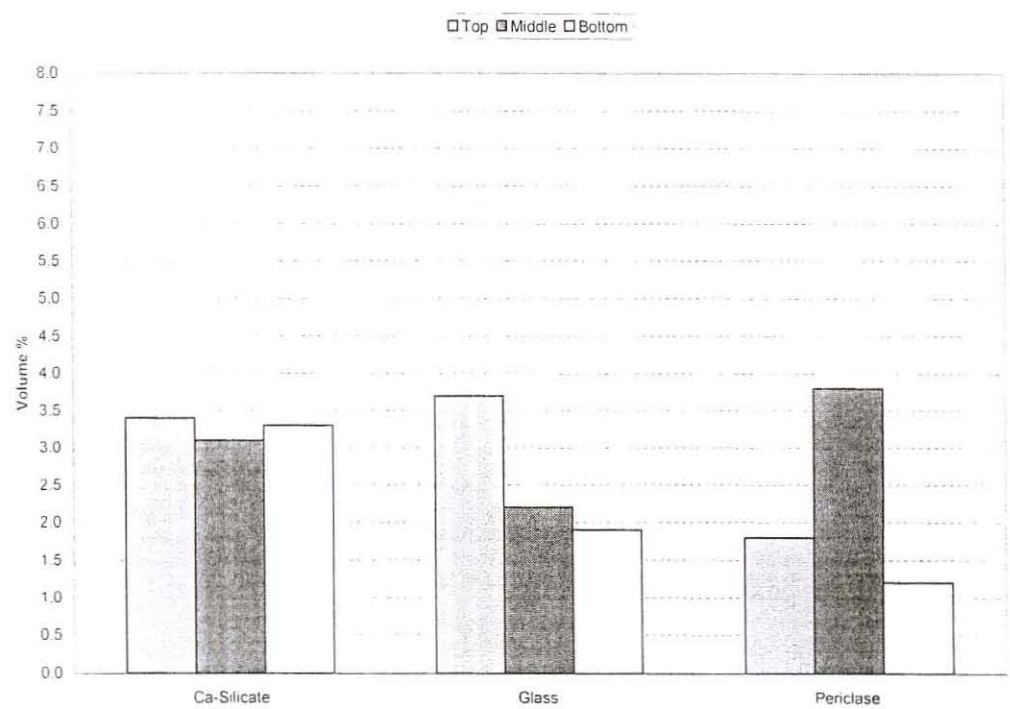

Glassy silicate, often referred to as slag phases, is formed when the melt from which primary phases have precipitated is rapidly cooled. The silicates can contain iron oxide as a substitute for calcium oxide and other impurities such as Al^{3+}, Mg^{2+} and other alkalines[3]. The calcium silicates are present as fine-grained lens shaped and/or dendritic crystals as shown in **Figure 28**. The calcium silicate is in general associated with SFCA and/or magnetite.

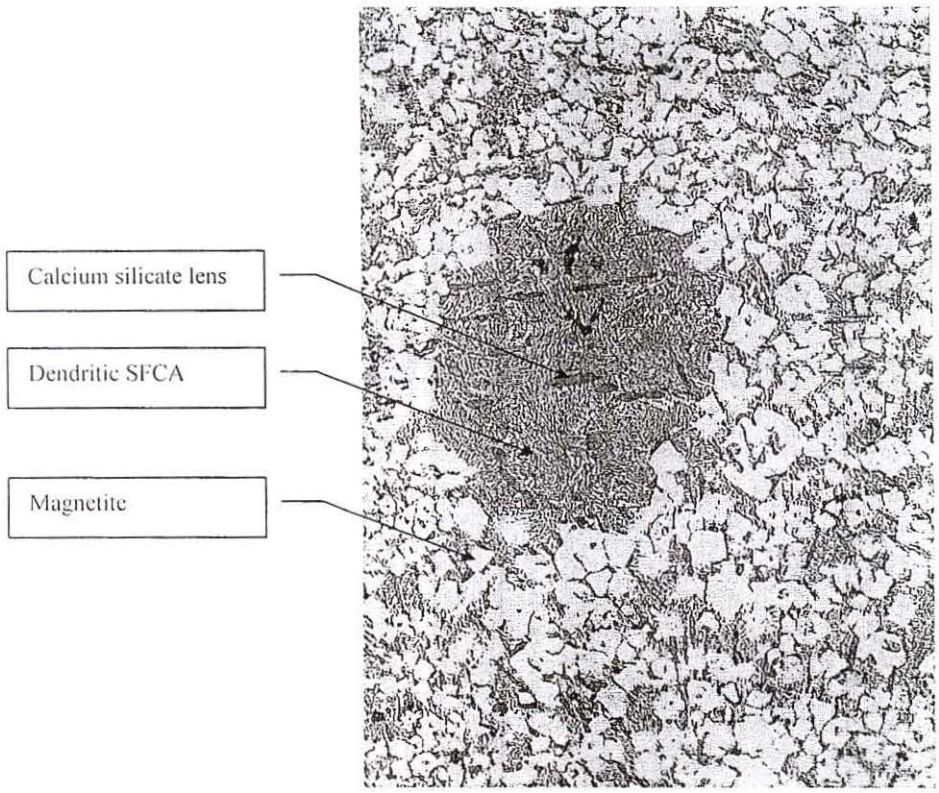

***Figure 28**: The calcium silicates are present as fine-grained lens shaped crystals. Dendritic SFCA and magnetite are embedded in a silicate rich glassy matrix (X 200).*

According to the chemical analyses data there are two different groups of calcium silicate present in the sinter produced in the sinter pot tests in both series. This difference is associated with the FeO content of the calcium silicate. In the first group the FeO content is lower than 10% while the FeO content of the second group is higher than 10% as shown in **Figure 29** and **Figure 30**.

Figure 29: Calcium silicate (Series 1)

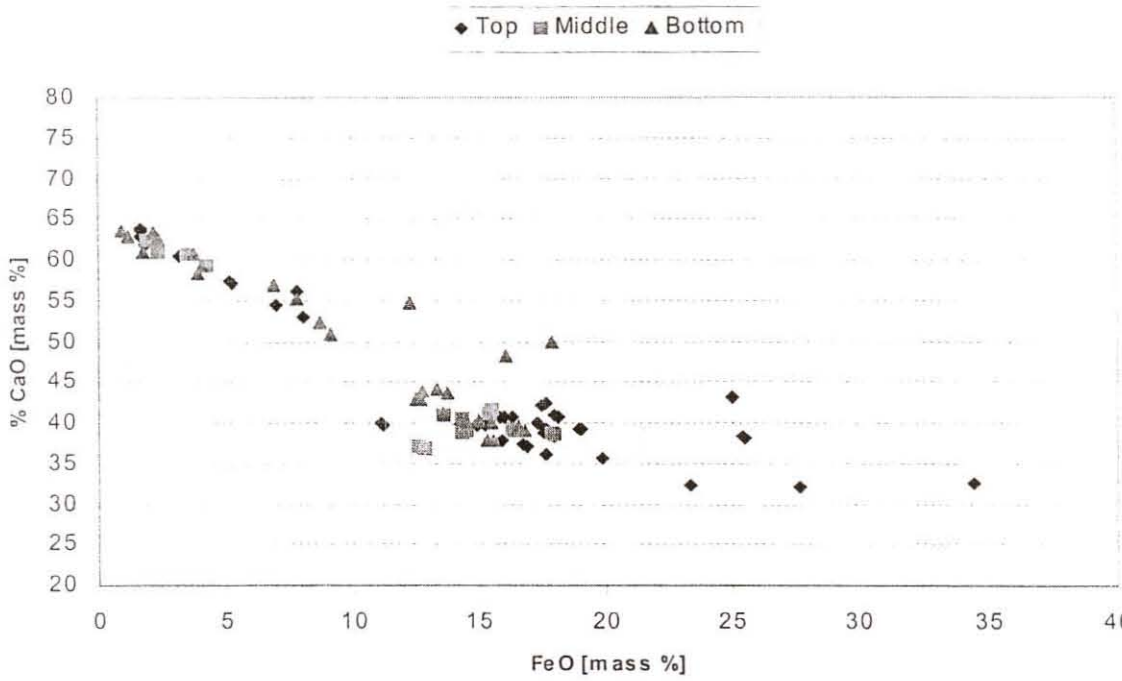

Figure 30: Calcium silicate (Series 2)

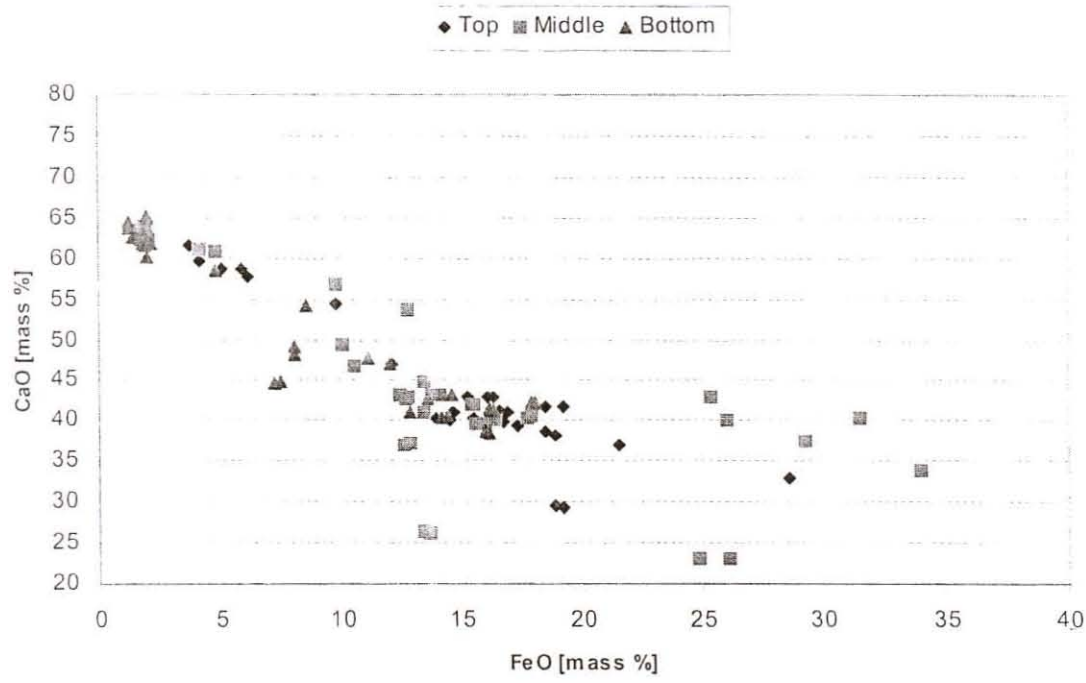

In the first group the FeO content is lower than 10% (**Table 13**). The typical CaO content is ±60% and the typical SiO_2 content is ±30%.

Table 13: Chemical analyses of the calcium silicate

(%FeO < 10%)

	Series1: 1100mmH_2O			Series 2: 1500mmH_2O		
	Top	**Middle**	**Bottom**	**Top**	**Middle**	**Bottom**
FeO	4.85	3.05	3.31	4.06	2.98	4.37
SiO_2	31.48	32.54	32.38	32.00	32.07	32.04
TiO_2	0.04	0.01	0.89	0.11	0.14	0.10
CaO	59.55	62.18	59.18	59.53	60.78	58.92
SO_3	0.07	0.04	0.43	0.10	0.10	0.15
MnO	0.05	0.08	0.05	0.08	0.05	0.07
K_2O	0.02	0.02	0.00	0.08	0.04	0.10
MgO	0.09	0.06	0.11	0.09	0.07	0.10
Al_2O_3	0.36	0.21	0.88	1.37	0.27	0.64
Na_2O	0.05	0.03	0.08	0.06	0.07	0.13
P_2O_5	1.11	0.99	0.49	1.65	2.79	0.88

Calcium oxide is replaced by iron oxide in the second group of calcium silicate. The FeO content is higher than 10% (**Table 14**). The typical CaO content changes to ±40% while the typical SiO_2 content remains at ±30%.

Table 14: Chemical analyses of the calcium silicate

(%FeO > 10%)

	Series1: 1100mmH_2O			Series 2: 1500mmH_2O		
	Top	**Middle**	**Bottom**	**Top**	**Middle**	**Bottom**
FeO	16.48	13.97	14.76	16.59	15.14	14.61
SiO_2	35.74	34.86	34.74	32.91	33.97	33.39
TiO_2	0.79	0.88	0.83	0.68	1.05	0.78
CaO	40.01	41.19	42.20	39.55	39.33	42.76
SO_3	0.10	0.08	0.18	0.16	0.08	0.12
MnO	0.18	0.24	0.13	0.21	0.28	0.16
K_2O	0.04	0.13	0.00	0.12	0.41	0.25
MgO	0.31	0.36	0.32	0.56	0.30	0.35
Al_2O_3	3.13	4.52	3.97	6.84	6.16	3.78
Na_2O	0.04	0.05	0.12	0.05	0.07	0.11
P_2O_5	0.32	0.27	0.32	0.49	0.56	0.81

5.6 CORRELATION BETWEEN PHASES AND SINTER QUALITY

Sinter quality is mainly governed by the microstructure of the sinter. Sinter is an aggregate of bonding phases, unmelted particles and pores. The bonding phases originate during the sintering process. Unmelted particles are mainly residual large ore particles and sometimes unreacted, residual flux particles.

The presence of magnetite results in the deterioration of the physical properties of the sinter. During cooling, internal tensions are developed because of the difference in shrinkage of the phases. In the case of magnetite this phenomenon is sufficient to produce cracks. Hematite is usually free of cracks, except in the areas where magnetite is precipitated. According to the literature, magnetite is the major source of crack formation and poor physical properties of the sinter[4][12].

From the results of this investigation, a strong relation between the magnetite content and sinter strength could not be found (**Figure 31**).

Figure 31: Magnetite content versus Tumbler index.

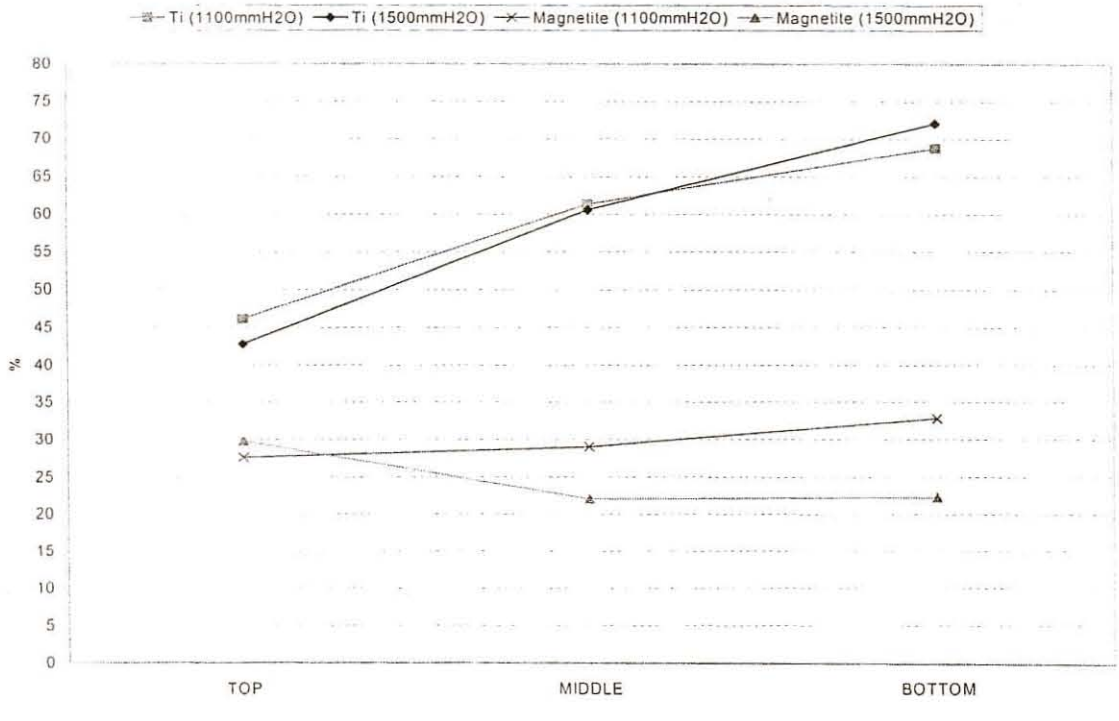

The total SFCA content increases from the top layer to the bottom layer as does the tumbler index. This correlation is shown in **Figure 32**.

Figure 32: SFCA content versus Tumbler index.

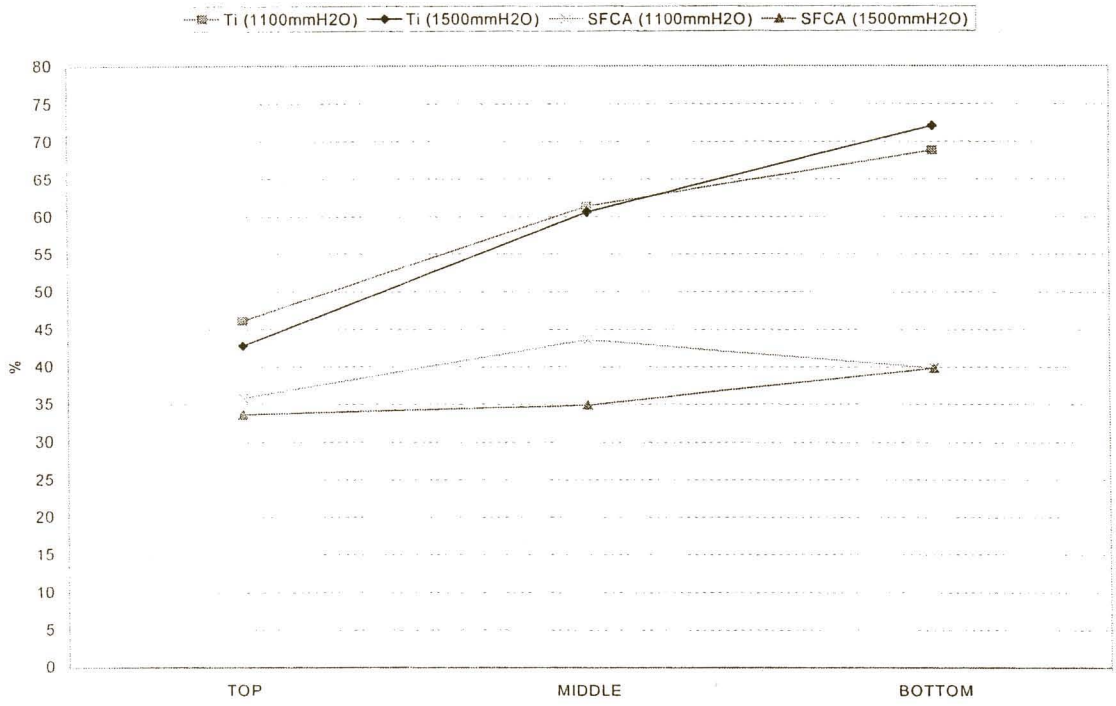

SFCA results in the improvement of the physical properties of the sinter. The bonding phases make up the majority of phases within sinter (up to 80vol%). The sinter properties are therefore strongly related to the bonding phases. The phases are formed during the sinter process at temperatures above 1100°C. SFCA is the most important bonding phase in the sinter and therefore improves the physical properties of the sinter. This is clearly illustrated when the SFCA content of the bottom layer of series one decreases the tumbler index also decreases (**Figure 32**).

The glass content of the sinter decreases from the top layer to the bottom layer while the tumbler index increases from the top layer to the bottom layer. This correlation is shown in **Figure 33**. Glass results in the deterioration of the physical properties of the sinter. The degree of breakage depends on the ease with which cracks propagate through the sinter particle. Glass is not a very strong bonding phase. Cracks will easily propagate through this phase resulting in poor physical properties.

Figure 33: Glass content versus Tumbler index.

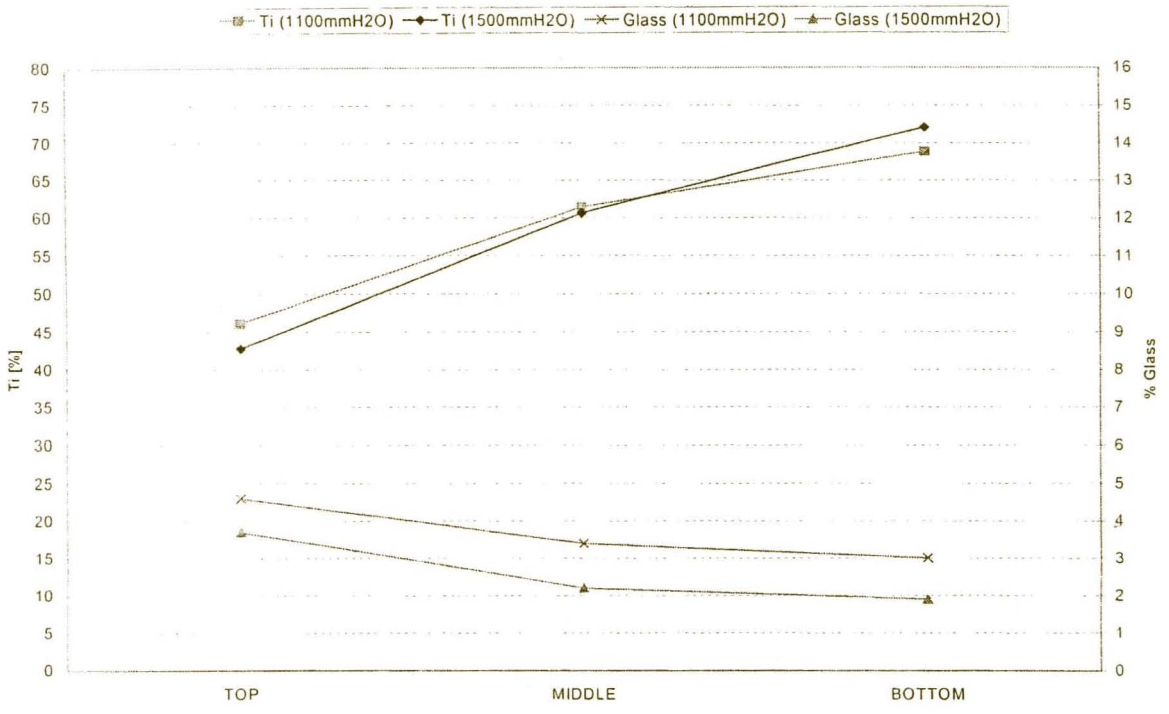

6. CONCLUSIONS

It is possible to change the temperature-time-characteristics of the sinter process by changing the airflow rate through the sinter bed. The air flow rate increased when the pressure drop over the sinter bed was increased. The rate of downward movement through the sinter bed of the combustion zone increased as a result. This was indicated by a shorter sintering time as well as different temperature profiles in the different sinter layers.

The sintering time at temperatures above 1100°C is related to the airflow rate through the sinter bed. The higher the airflow rate, the shorter the sintering time at temperatures above 1100°C. By changing the temperature-time-characteristics of the sinter process it is possible to control the sintering time at temperatures above 1100°C. The sintering time above 1100°C increased from the top layer to the bottom layer in the sinter bed.

The temperature-time-characteristics of the sinter process have a major influence on phase formation during the sinter process. The phase composition differs in each layer because each layer is subjected to different temperature-time-characteristics. This study revealed that the main constituents of the sinter were hematite, magnetite and SFCA with small quantities of calcium silicate, glass, periclase, wustite and manganosite.

The sintering time above 1100°C is one of the most important parameters to ensure that phases to enhance sinter quality are formed. At a lower airflow rate the sintering time at temperatures above 1100°C increases resulting in a higher SFCA content. The sintering time at temperatures above 1100°C increased from the top layer to the bottom layer resulting in a higher SFCA content in the middle and bottom layers.

Magnetite has a detrimental influence on the physical properties of the sinter. From the results of this investigation, a strong relation between the magnetite content and sinter strength could not be found.

SFCA results in the improvement of the physical properties of the sinter. In this study the total SFCA content increases from the top layer to the bottom layer and the physical properties improved from the top layer to the bottom layer.

Glass results in the deterioration of the physical properties of the sinter. The glass content of the sinter decreases from the top layer to the bottom layer while the physical properties improved from the top layer to the bottom layer.

In spite of the correlation found between the sinter strength and phases of the sinter in this investigation, it became clear that the phases are not the only parameter determining the sinter strength. The morphology of the sinter phases present, porosity of the sinter and coke rate may have an influence on the sinter quality and should be investigated.

In practice it is important to find an optimum between the airflow rate, sinter quality as well as production rate.

7. BIBLIOGRAPHY

1. Loo, CE. Et. al. Influence of material properties on high-temperature zone reactions in sintering of iron ore. *Transactions of the Institute of Mining and Metallurgy,* 101, January-April. 1992. pp. C7-C16.
2. Sasaki, M. et al. Consideration on the properties of sinter from the point of view of sintering reactions. *Nippon Steel Corporation Tetsu-to-Hagane,* vol. 68. 1982. p.563-598.
3. Cappel, F. The history and development of iron ore sintering. *Ironmaking Conference Proceedings*, vol. 50. 1991. pp.525 – 539.
4. Dawson, PR. Research studies on sintering and sinter quality. *Ironmaking and Steelmaking,* vol. 20. no. 2. 1993. pp.137-143.
5. Loo, CE. Some progress in understanding the science of iron ore sintering. *ISTI Ironmaking Conference Proceedings.* 1998. pp. 1299-1316.
6. Davies, W. Some practical applications of fundamental sinter research. *Canadian Mining and Metallurgical Transactions,* vol. LXIII. 1960. pp. 114-126.
7. Wendeborn H.B. Sintering as a physical process. *Journal of the Iron and Steel Institute,* vol. 175. November 1953. pp. 280-288.
8. Li-Heng Hsieh et. al. Sintering conditions for simulating the formation of mineral phases in industrial iron ore sinter. *ISIJ International.* vol. 29. no. 1. 1989. pp. 24-32.
9. Dawson P.R. et. al. The influence of the sintering temperature profile on the mineralogy and properties of iron ore sinters. *Proc. Australas. Inst. Min. Metall.* no. 289. June/July, 1984. pp. 163-169.
10. Li-Heng Hsieh et. al. Effect of oxygen potential on mineral formation in lime fluxed iron ore sinter. *ISIJ International.* vol. 29. no. 8. 1989. pp. 625-634.
11. Loo, CE. et. al. Assimilation of large ore and flux particles in iron ore sintering. *Transactions of the Institute of Mining and Metallurgy,* 101, May-August. 1992. pp. C105-C117.
12. Mukherjee, T. et. al. Structure of fluxed sinter. *Iron and steelmaking* 1985. vol. 12 no. 4 pp. 151-C155.
13. Botha, PA. 'n Mineralogiese benadering tot die optimisering van sintergehalte. *PhD tesis, Universiteit van Pretoria.* 1990.
14. Dawson, PR. et. al. Influence of alumina on development of complex calcium ferrites in iron ore sinters. *Transactions of the Institute of Mining and Metallurgy,* 94, June. 1985. pp. C71-C78.

15. Ponghis, N. and Poos, A. Investigation on the mechanisms governing iron ore sintering. *CRM Liege – Belgium.* pp. 91-101.

16. Bristow, NJ. and Waters, AG. Role of SFCA in promoting high-temperature reduction properties of iron ore sinters. *Transactions of the Institute of Mining and Metallurgy,* 100, January-April. 1991. pp. C1-C10.

17. Chaigneau, R. Complex calcium ferrites in the blast furnace process. *Thesis. Delft University.* Delft. 1994.

18. Li-Heng Hsieh et. al. Effect of raw material composition on the mineral phases in lime-fluxed iron ore sinter. *ISIJ International.* vol. 33. no. 4. 1993. pp. 462-473.

APPENDIX A: PHYSICAL PROPERTIES

Test series	Note	Series 1	Series 1	Series 1	Series 2	Series 2	Series 2
Layer		TOP	MIDDLE	BOTTOM	TOP	MIDDLE	BOTTOM
Reference		MIN31	MIN32	MIN33	MIN12	MIN13	MIN14
Pressure drop [mmH2O]		1100	1100	1100	1500	1500	1500
Tumbler test							
Tumbler index %+6.30mm	1	46.12	61.39	68.80	42.80	60.60	72.10
Tumbler index %-6.30+0.50mm	2	49.89	34.00	26.50	53.30	35.10	23.30
Abrasive index %-0.50mm	3	3.99	4.61	4.70	3.90	4.30	4.60
Sieve analyses (%)							
+40		1.40	6.23	14.90	0.00	2.55	5.01
-40+25		4.66	18.97	24.20	3.27	13.00	10.49
-25+16		18.72	27.30	24.53	12.56	29.73	19.15
-16+12.5		13.33	11.98	9.15	12.41	12.90	16.78
-12.5+10		11.60	7.75	6.60	12.52	9.47	11.49
-10+5		32.88	16.49	12.11	39.64	20.92	23.23
-5		17.42	11.27	8.52	19.59	11.43	13.85
Mean particle size							
Mean particle size [mm]		11.97	18.37	22.41	10.20	15.96	15.18
Mean particle size [mm] of +5mm fraction		13.75	20.25	24.17	11.82	17.57	17.05

Notes:

1. Std. Deviation: 0.32%
2. Std. Deviation: 0.31%
3. Std. Deviation: 0.13%

APPENDIX B: CHEMICAL ANALYSIS (%)

Test series	Note	Series 1	Series 1	Series 1	Series 2	Series 2	Series 2
Layer		TOP	MIDDLE	BOTTOM	TOP	MIDDLE	BOTTOM
Reference		MIN31	MIN32	MIN33	MIN12	MIN13	MIN14
Pressure drop [mmH2O]		1100	1100	1100	1500	1500	1500
Fe(tot)	1	53.30	53.20	52.80	52.10	52.30	52.50
Fe(met)	1	0.25	0.12	0.07	0.01	0.03	0.03
FeO	1	6.55	6.82	6.99	6.02	6.49	6.59
Fe2O3	1	68.60	68.30	67.60	67.80	67.50	67.60
CaO	1	11.90	12.10	12.40	12.50	12.50	12.60
MgO	1	2.66	2.75	2.78	2.71	2.72	2.74
SiO2	1	6.03	6.12	6.33	5.81	5.88	5.88
Al2O3	1	1.93	2.03	2.10	2.04	2.06	2.02
K2O	1	0.04	0.03	0.04	0.10	0.08	0.08
Na2O	1	0.04	0.04	0.04	0.02	0.02	0.02
MnO	1	1.34	1.24	1.31	1.34	1.29	1.28
TiO2	1	0.13	0.13	0.15	0.12	0.13	0.12
P	1	0.05	0.06	0.06	0.07	0.08	0.07
S	1	0.030	0.020	0.020	0.025	0.025	0.022
C	1	0.31	0.25	0.16	0.23	0.20	0.26
CaO/SiO2		1.97	1.98	1.96	2.15	2.13	2.14

Notes:

1. Std. Deviation: 0.5%

APPENDIX C: PHASE ANALYSIS (vol%)

Test series	Note	Series 1	Series 1	Series 1	Series 2	Series 2	Series 2
Layer		TOP	MIDDLE	BOTTOM	TOP	MIDDLE	BOTTOM
Reference		MIN31	MIN32	MIN33	MIN12	MIN13	MIN14
Pressure drop [mmH2O]		1100	1100	1100	1500	1500	1500
Magnetite	1	27.60	29.00	32.80	29.80	22.00	22.20
Massive Hematite	1	18.60	8.60	8.60	19.40	26.00	23.60
Crystalline Hematite	1	6.60	9.00	6.60	7.20	6.90	6.70
Secondary Hematite	1	0.20	0.60	0.20	0.10	0.10	0.20
Total Hematite		25.40	18.20	15.40	26.70	33.00	30.50
Columnar SFCA	1	5.80	10.80	8.40	3.00	4.00	7.30
Acicular SFCA	1	24.60	28.80	26.40	25.80	26.50	30.20
Dendritic SFCA	1	5.40	4.00	5.00	4.80	4.40	2.30
Total SFCA		35.80	43.60	39.80	33.60	34.90	39.80
Ca-Silicate	2	3.00	5.00	6.80	3.40	3.10	3.30
Glass	2	4.60	3.40	3.00	3.70	2.20	1.90
Periclase	2	2.40	0.60	2.00	1.80	3.80	1.20
Wustite	2	1.00	0.00	0.00	0.10	0.20	0.20
Manganosite	2	0.20	0.20	0.20	0.40	0.50	0.10

Notes:
1. Std. Deviation: 1.0%
2. Std. Deviation: 0.5%

Magnification: 40x
More than 1000 points counted over sample area in steps of 2um.

APPENDIX D: HEMATITE - HYPOTHESIS TESTS

HEMATITE SERIES 2 (1500mmH2O)

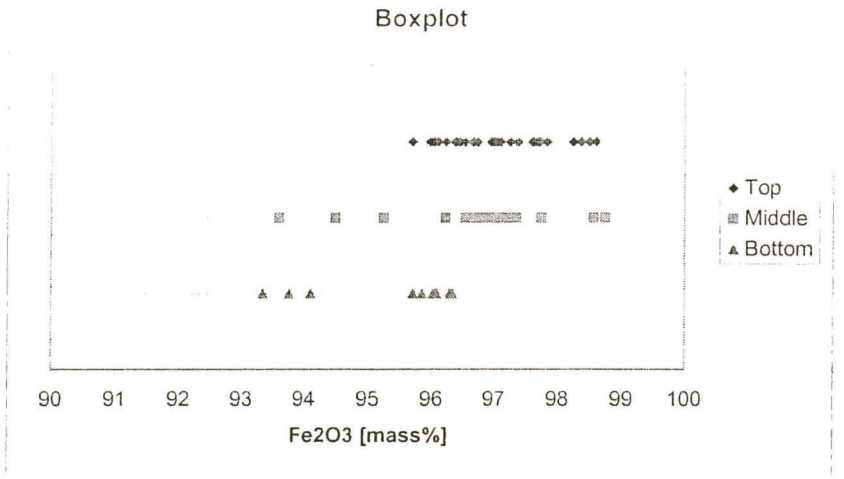

Anova: Single Factor

SUMMARY

Groups	*Count*	*Sum*	*Average*	*Variance*
Top	28	2716.886	97.03163	0.669867
Middle	25	2392.743	95.70974	14.6318
Bottom	10	953.5019	95.35019	1.31748

ANOVA

Source of Variation	*SS*	*df*	*MS*	*F*	*P-value*	*F crit*
Between Groups	32.49411	2	16.24706	2.557873	0.085893	3.150411
Within Groups	381.107	60	6.351784			
Total	413.6011	62				

Hypothesis Test
Ho: a1=a2=a3
Reject Ho if F > F crit
F < F crit : a1=a2=a3
Therefore, there is not a difference in the mean Fe2O3 content of the different samples

HEMATITE SERIES 1 (1100mmH2O)

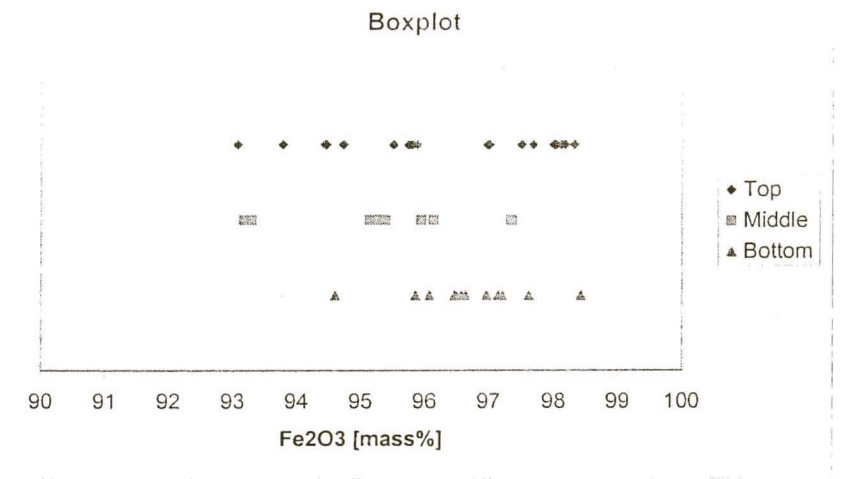

Anova: Single Factor

SUMMARY

Groups	*Count*	*Sum*	*Average*	*Variance*
Top	21	2033.004	96.80971	4.376214
Middle	10	954.2147	95.42147	2.001166
Bottom	12	1159.979	96.66489	0.904577

ANOVA

Source of Variation	*SS*	*df*	*MS*	*F*	*P-value*	*F crit*
Between Groups	13.84959	2	6.924797	2.398507	0.103805	3.231733
Within Groups	115.4851	40	2.887128			
Total	129.3347	42				

Hypothesis Test
Ho: a1=a2=a3
Reject Ho if F > F crit
F < F crit : a1=a2=a3
Therefore, there is not a difference in the mean Fe2O3 content of the different samples

APPENDIX E: MAGNETITE - HYPOTHESIS TESTS

MAGNETITE SERIES 1 (1100mmH2O)

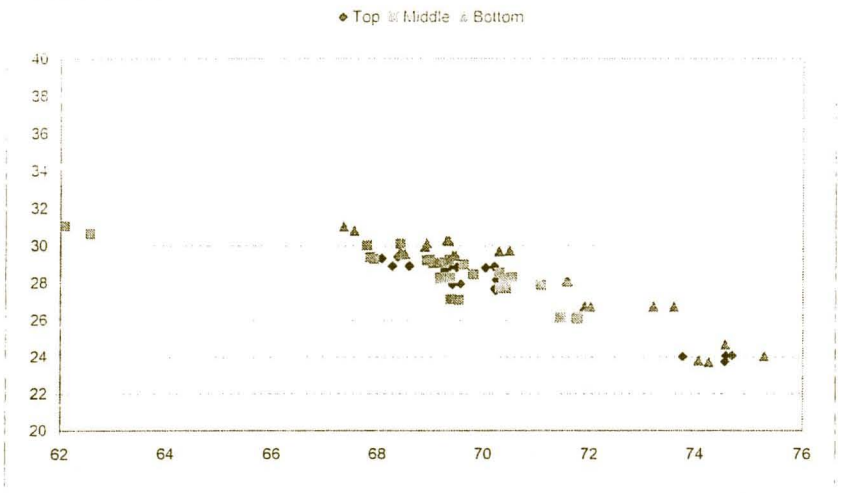

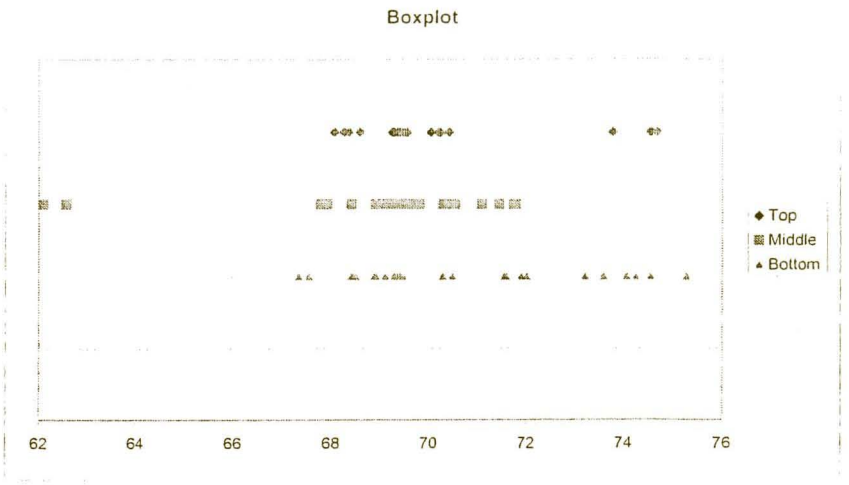

Anova: Single Factor

SUMMARY

Groups	*Count*	*Sum*	*Average*	*Variance*
Top	20	1408.525	70.42624	4.650113
Middle	30	2077.683	69.25609	4.769674
Bottom	26	1835.124	70.58169	5.533724

ANOVA

Source of Variation	*SS*	*df*	*MS*	*F*	*P-value*	*F crit*
Between Groups	29.0099	2	14.50495	2.900865	0.061338	3.122103
Within Groups	365.0158	73	5.000216			
Total	394.0257	75				

Hypothesis Test
Ho: a1=a2=a3
Reject Ho if F > F crit
F < F crit : a1=a2=a3
Therefore, there is not a difference in the mean Fe2O3+Al2O3 content of the different samples

APPENDIX E: MAGNETITE - HYPOTHESIS TESTS (continues)

MAGNETITE SERIES 2 (1500mmH2O)

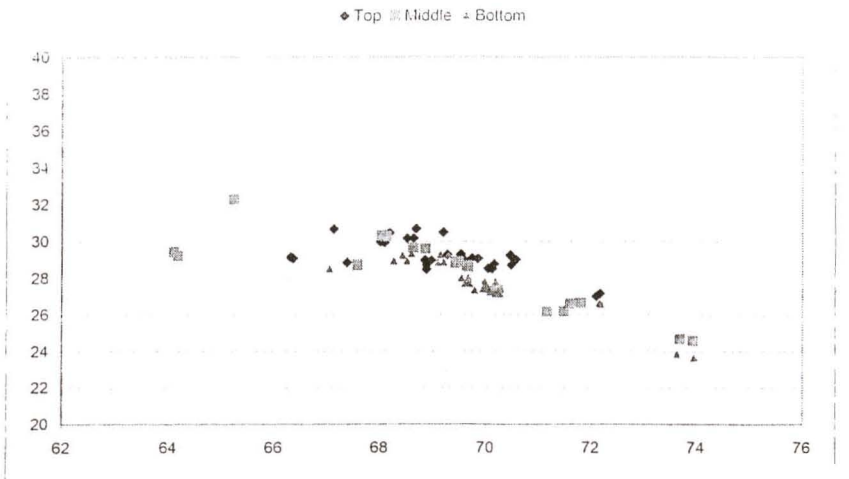

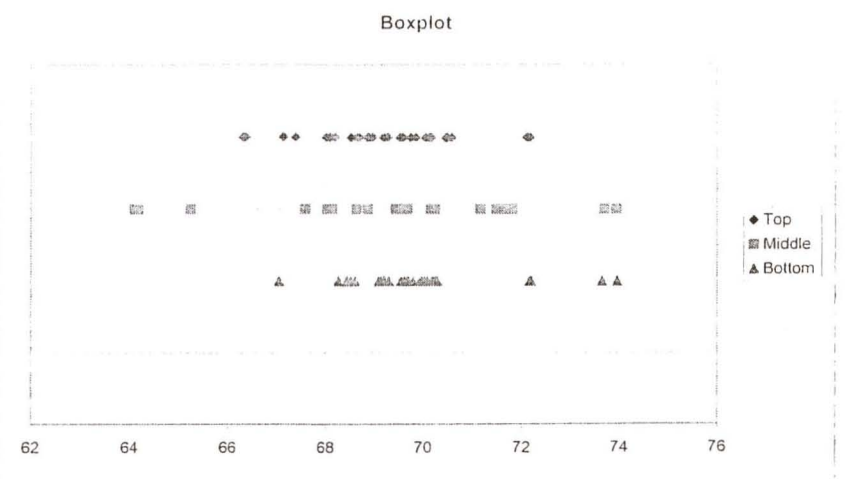

Anova: Single Factor

SUMMARY

Groups	*Count*	*Sum*	*Average*	*Variance*
Top	29	2005.774	69.16463	1.963918
Middle	21	1454.647	69.26889	7.092478
Bottom	30	2098.603	69.95344	2.08457

ANOVA

Source of Variation	*SS*	*df*	*MS*	*F*	*P-value*	*F crit*
Between Groups	10.53972	2	5.269862	1.577117	0.213169	3.11536
Within Groups	257.2918	77	3.341452			
Total	267.8315	79				

Hypothesis Test
Ho: a1=a2=a3
Reject Ho if F > F crit
F < F crit : a1=a2=a3
Therefore, there is not a difference in the mean Fe2O3+Al2O3 content of the different samples

APPENDIX F: SFCA - HYPOTHESIS TESTS

SFCA SERIES 1 (1100mmH2O)

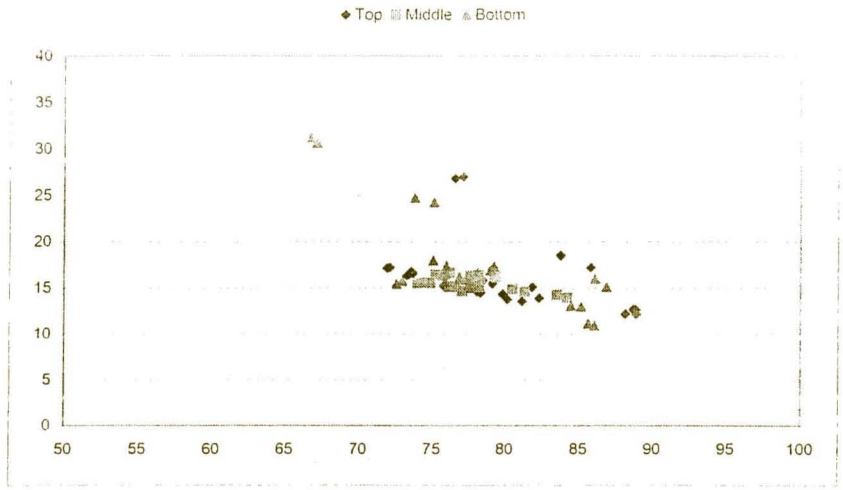

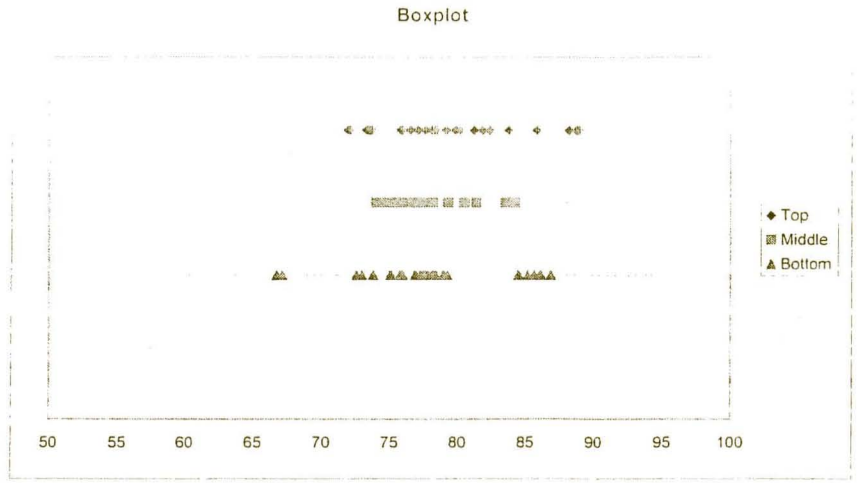

Anova: Single Factor

SUMMARY

Groups	*Count*	*Sum*	*Average*	*Variance*
Top	27	2142.469	79.3507	27.61653
Middle	22	1706.81	77.58228	7.811781
Bottom	32	2429.356	75.91737	74.80208

ANOVA

Source of Variation	*SS*	*df*	*MS*	*F*	*P-value*	*F crit*
Between Groups	172.7611	2	86.38056	2.104907	0.128726	3.113797
Within Groups	3200.942	78	41.03771			
Total	3373.703	80				

Hypothesis Test
Ho: a1=a2=a3
Reject Ho if F > F crit
F < F crit : a1=a2=a3
Therefore, there is not a difference in the mean Fe2O3+Al2O3 content of the different samples

APPENDIX F: SFCA - HYPOTHESIS TESTS (continues)

SFCA SERIES 2 (1500mmH2O)

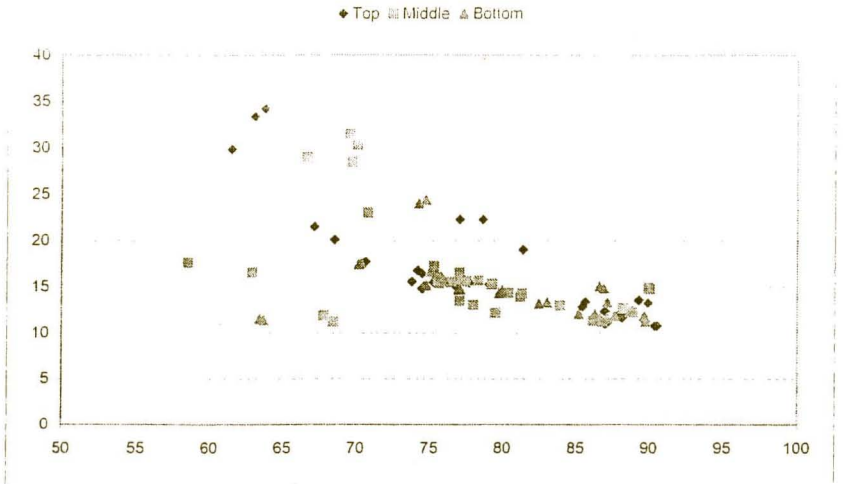

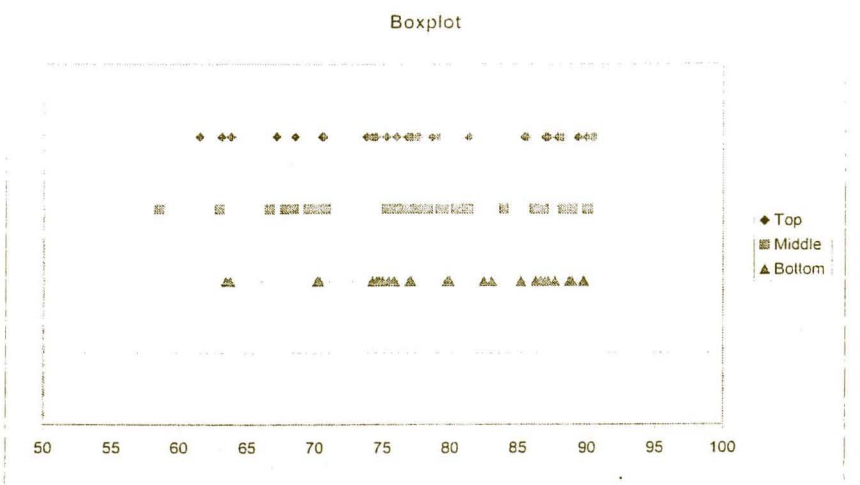

Anova: Single Factor

SUMMARY

Groups	*Count*	*Sum*	*Average*	*Variance*
Top	33	2594.438	78.61933	72.88107
Middle	34	2628.629	77.31261	60.43059
Bottom	31	2486.372	80.20554	58.66641

ANOVA

Source of Variation	*SS*	*df*	*MS*	*F*	*P-value*	*F crit*
Between Groups	135.8235	2	67.91176	1.060006	0.350515	3.092218
Within Groups	6086.396	95	64.06733			
Total	6222.219	97				

Hypothesis Test
Ho: a1=a2=a3
Reject Ho if F > F crit
F < F crit : a1=a2=a3
Therefore, there is not a difference in the mean Fe2O3+Al2O3 content of the different samples

APPENDIX G: EXAMPLES OF CALCULATIONS

TABLE A: Chemical analyses: Mass percentage

	Fe2O3	FeO	SiO2	TiO2	CaO	SO3	MnO	K2O	MgO	Al2O3	Na2O	P2O5	Total
Hematite	-	86.60	0.00	0.27	0.34	0.00	0.06	0.00	0.00	1.05	0.00	0.00	88.34
Magnetite	-	84.21	0.02	0.01	2.14	0.00	1.08	0.00	3.21	1.43	0.00	0.00	92.11
SFCA	-	65.46	7.85	0.09	15.02	0.00	0.24	0.00	0.54	3.53	0.00	0.01	92.74

TABLE B: Calculated chemical analyses: Mass percentage

	Fe2O3	FeO	SiO2	TiO2	CaO	SO3	MnO	K2O	MgO	Al2O3	Na2O	P2O5	Total
Hematite	96.00	0.00	0.00	0.27	0.34	0.00	0.06	0.00	0.00	1.05	0.00	0.00	97.74
Magnetite	69.51	21.39	0.02	0.01	2.14	0.00	1.08	0.00	3.21	1.43	0.00	0.00	98.80
SFCA	71.43	0.96	7.85	0.09	15.02	0.00	0.24	0.00	0.54	3.53	0.00	0.01	99.67

CALCULATIONS

Calculation of Fe2O3 in Hematite:

Step 1: mole Fe = mole FeO = %FeO / (56 + 16) = 86.60 / (56 +16) = 1.20
Step 2: 4 mole Fe reacts with 3 mole O2 resulting in 2 mole Fe2O3
Step 3: therefore, mole Fe2O3 = 0.5x mole Fe
Step 4: mole Fe2O3 = 0.5 x 1.20 = 0.6
Step 5: % Fe2O3 = mole Fe2O3 x 160 = 0.6 x 160 = 96
Step 6: Recalculate to give results of Hematite in Table B

Recalculation of Fe2O3 and FeO in Magnetite assuming a M3O4 structure

Step 1: Calculate the mole cations from the chemical analyses shown in TABLE A

mole cations = % MO / molar mass of MO

n Fe3+	n Fe2+	n Si4+	n Al3+	n Mg2+	n Ca2+	n Mn2+	Total
-	1.17	0.00	0.03	0.08	0.04	0.02	1.33

Step 2: Recalculate the mole cations to ensure that the sum of the cations equals 3

mole cations = (3 / 1.33) x mole cations calculated in step 1

n Fe3+	n Fe2+	n Si4+	n Al3+	n Mg2+	n Ca2+	n Mn2+	Total
-	2.63	0.00	0.06	0.18	0.09	0.03	3.00

Step 3: Determine the mole oxygen anions associated with the cations as calculated in step 2

mole oxygen anions associated with:

n Fe3+	n Fe2+	n Si4+	n Al3+	n Mg2+	n Ca2+	n Mn2+	Total
-	2.63	0.00	0.09	0.18	0.09	0.03	3.02

Step 4: Fe3+ cations is present if the total mole oxygen anions calculated in step 3 is less than four.

Step 5: mole Fe3+ cations = 2 x (4 - total mole oxygen anions) = 2 x (4 - 3.02) = 1.96

Step 6: %Fe2O3 = (mole Fe3+ cations x total mole cations / 3) x 160 x 0.5
therefore, %Fe2O3 = 1.96 x 1.33 / 3 x 160 x 0.5 = 69.51

Step 7: mole Fe2+ cations = mole Fe2+ cations calculated in step 3 - mole Fe3+ cations = 2.63 - 1.96 = 0.67

Step 8: %FeO = (mole Fe2+ cations x total mole cations / 3) x 72
therefore, %FeO = 0.67 x 1.33 / 3 x 72 = 21.39

Step 9: Recalculate to give results of the chemical analyses of Magnetite in Table B

Step 10: Accordingly, Magnetite Stoichiometry (XY2O4) = (Fe,Mg,Si,Ca,Mn) (Fe,Al)2 O4

i Fe2+	i Mg2+	i Si4+	i Ca2+	i Mn2+		i Fe3+	i Al3+		i O2-
0.67	0.18	0.00	0.09	0.03	1.00	1.96	0.06	2.00	4.00

Recalculation of Fe2O3 and FeO in SFCA assuming a M25O36 structure

Step 1: Calculate the mole cations from the chemical analyses shown in TABLE A

mole cations = % MO / molar mass of MO

n Fe3+	n Fe2+	n Si4+	n Al3+	n Mg2+	n Ca2+	n Mn2+	Total
-	0.91	0.13	0.07	0.01	0.27	0.00	1.39

Step 2: Recalculate the mole cations to ensure that the sum of the cations equals 25

mole cations = (25 / 1.39) x mole cations calculated in step 1

n Fe3+	n Fe2+	n Si4+	n Al3+	n Mg2+	n Ca2+	n Mn2+	Total
-	16.30	2.35	1.24	0.24	4.81	0.06	25.00

Step 3: Determine the mole oxygen anions associated with the cations as calculated in step 2

mole oxygen anions associated with:

n Fe3+	n Fe2+	n Si4+	n Al3+	n Mg2+	n Ca2+	n Mn2+	Total
-	16.30	4.70	1.86	0.24	4.81	0.06	27.97

Step 4: mole Fe3+ cations = 2 x (36 - total mole oxygen anions) = 2 x (36 - 27.97) = 16.06

Step 5: %Fe2O3 = (mole Fe3+ cations x total mole cations / 25) x 160 x 0.5
therefore, %Fe2O3 = 16.06 x 1.39 / 25 x 160 x 0.5 = 71.43

Step 6: mole Fe2+ cations = mole Fe2+ cations calculated in step 3 - mole Fe3+ cations = 16.30 - 16.06 = 0.24

Step 7: %FeO = (mole Fe2+ cations x total mole cations / 25) x 72
therefore, %FeO = 0.24 x 1.39 / 25 x 72 = 0.96

Step 8: Recalculate to give results in Table B

Step 9: Accordingly, SFCA Stoichiometry (M25O36) = Ca5,Si2,(Fe,Al)18 O4

i Fe2+	i Mg2+	i Si4+	i Ca2+	i Mn2+		i Fe3+	i Al3+		i O2-
0.24	0.24	2.35	4.81	0.06	7.70	16.06	1.24	17.30	36.00